22
Gas Separation by Zeolites

Shivaji Sircar
Lehigh University, Bethlehem, Pennsylvania, U.S.A.

Alan L. Myers
University of Pennsylvania, Philadelphia, Pennsylvania, U.S.A.

I. INTRODUCTION

Separation and purification of gas mixtures by selective adsorption of one or more of its components on a micro- or mesoporous solid adsorbent is a major unit operation in the chemical, petrochemical, environmental, medical, and electronic gas industries. Figure 1 demonstrates the phenomenal growth in this technology (1). It shows that the total number of U.S. patents granted between the years of 1980 and 2000 on "gas separation by adsorption" and "adsorption for air pollution control" are more than 3000 and 1000, respectively. The figure also shows that the patent estate in these areas is growing rapidly. The main reasons are as follows:

- Commercial availability of a spectrum of porous adsorbents (zeolites, activated carbons, silica and alumina gels, polymeric sorbents, etc.) which offer many different choices of core adsorptive properties (equilibria, kinetics, and heats) for a given gas separation or purification application.
- Immense flexibility in the design and operation of adsorptive separation and purification processes using these adsorbents.

Since a successful adsorptive process is a good marriage of the optimal adsorbent with an efficient process design, there can be many different paths or combinations of materials and process schemes that satisfy the same separation criteria. The infinite variety of combinations is the driving force for innovations (1,2).

Unquestionably, zeolitic adsorbents have played a major role in the development of adsorption technology. Table 1 is a list of typical applications of zeolites. The three major areas of applications are:

1. Removal of trace or dilute impurities from a gas
2. Separation of bulk gas mixtures
3. Gas analysis

Category 1 is the traditional use of zeolitic adsorbents. Gas drying, desulfurization, and removal of toxic, corrosive, and heavier organic compounds from a contaminated gas are primary examples. Numerous types of industrial gases containing various kinds of impurities are treated by adsorption on zeolites (1–11). Category 2 applications for zeolites are more recent developments. The trend is to increase the product purity and

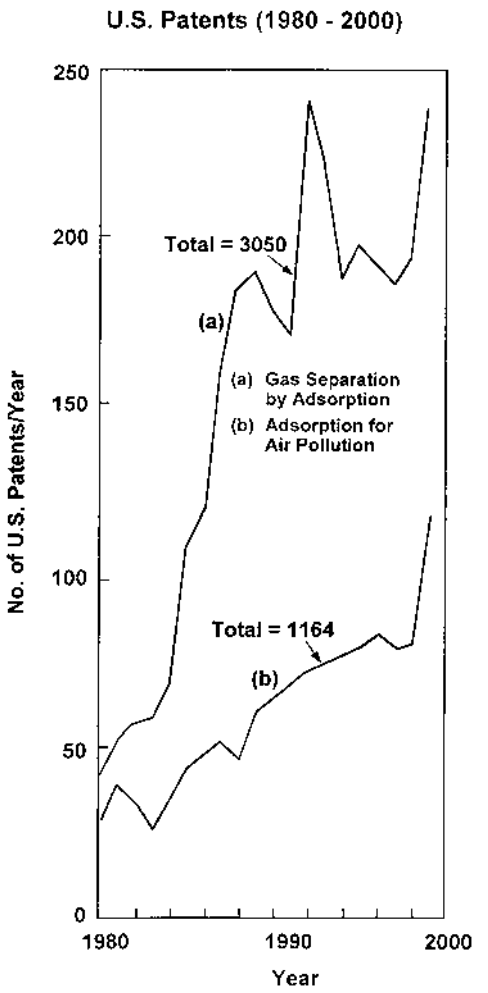

Fig. 1 U.S. patent survey for 1980–2000.

recovery and to increase the scale of application while lowering the overall energy requirement and cost for the separation. The most important example of category 3 is gas chromatography, which is used extensively as an analytical tool for research and process control.

The adsorptive processes for categories 1 and 2 are designed to pass a feed gas mixture through a column packed with a zeolite (or several different zeolites in layers) in order to produce a product enriched in the more weakly adsorbed component followed by desorption of the strongly adsorbed component so that zeolite can be reused. Thus, these separation schemes are unsteady-state cyclic processes. In a conventional thermal swing adsorption (TSA) process, the desorption step is carried out by heating the zeolite with a portion of the primary product gas. In a conventional pressure swing adsorption (PSA) process, the desorption is achieved by lowering the partial pressures of the adsorbed components in the gas phase (a) by reducing the total pressure in the adsorber and (b) by flowing a part of the primary product gas over the zeolite bed without heating. Numerous variations of these two generic process concepts have been proposed for improving the

Table 1 Applications of Zeolites for Gas Separation and Purification[a]

Trace or dilute impurity removal	Bulk gas separation	Gas analysis
Industrial gas drying (A,X)	Industrial production of O_2 and N_2 from air (A, X, mordenite)	Gas chromatography (A, X, mordenite)
Dehydration of air contained between double walls or windows (A)	Production of O_2 for medical use (A, X)	
Drying of acid gases (chabazite, mordenite)	Hydrogen production from steam-methane reforming off-gas and refinery off-gas (A, X)	
Desulfurization of gases (H_2S, COS, and mercaptans) (A)	CO_2-CH_4 separation from landfill gas (X)	
Solvent vapor recovery (A, X)	Alcohol dehydration (A, X)	
Removal of silanes from metal hydrides, hydrocarbons, and acid gases (A, mordenite)	Separation of straight-chain hydrocarbons from branched-chain and aromatic hydrocarbons (A)	
Removal of trace radioactive rare (Ar, Kr, Xe) gases (A)		
Trapping of Hg vapor, SO_2, NO_x (mordenite)		
Removal of SO_2, NO_x, HCl (mordenite)		
Deodorizing and air freshening (chabazite, clinoptilolite)		
Air pollution control (A, X)		
Removal of trace NH_3 (A, clinoptilolite)		

[a] Commonly used zeolite types in parentheses.

product quality and the overall separation efficiency, and for producing multiple products in a single-unit operation.

Category 1 applications are generally served by TSA processes except for the cases of gas drying and solvent vapor recovery, for which both TSA and PSA processes are used. Category 2 applications are exclusively served by PSA processes.

Although there are more than 40 different types of naturally occurring zeolite structures from volcanic sources, and most of them and at least 150 new synthetic types are available, the commonly used zeolites for all gas separation and purification applications listed in Table 1 are limited to synthetic zeolites types A and X, mordenite, chabazite, and clinoptilolite (3–9), which are very hydrophilic and polar materials.

Table 2 lists some of the crystallographic and physical properties of the commonly used zeolites (3). They provide a variety of pore openings, cavity and channel sizes, and framework Si/Al ratio. They are also available in various cation-exchanged (partial or complete) forms listed in Table 2. The type X framework is also produced with a lower Si/Al ratio (1.0 compared to 1.25 for normal X type), which can provide a higher concentration of cations in the crystal than the normal X type. This variety is called low-silica X (LSX) zeolite.

Table 2 Physical Properties of Zeolites[a] Used Commercially

Zeolite	Crystal framework Si/Al ratio	Crystal structure symmetry	Crystal density[b] (g/cm^3)	Common ion-exchanged forms	Pellet density (g/cm^3)	Bulk density (g/cm^3)	Nominal pore opening (A)
A	0.7–1.2	Cubic	1.52	Na,K,Ag, Mg,Ca	1.20	0.72	3,4,5
X	1.0–1.5	Cubic	1.47	Na,Li, Ca,Ba	1.05	0.65	7.5(NaX) 10.0(CaX)
Mordenite (small port)	4.5–5.0	Orthorhombic	1.83	Na,H,Ca	1.39	0.88	4
Chabazite	1.6–3.0	Trigonal	1.67	Na,Ca	1.16	0.73	4.9
Clinoptilolite	4.2–5.2	Monoclinic	1.85	K,Ca	—	—	3.5
Silicalite	very high	Orthorhombic	1.79	none	—	—	5.3

[a] All of these structures (Na form) are thermally stable up to at least 600°C.
[b] Dehydrated Na form.

The highly siliceous ($Si/Al \rightarrow \infty$) silicalite, which has no ion-exchange capacity and is nonpolar and hydrophobic, is also produced commercially. Although separations using silicalite have not yet been commercialized, a significant amount of research has recently been performed aiming to produce silicalite membranes that can efficiently separate xylene isomers. For more information on this, see Chapter 17 by Nair and Tsapatsis in this volume. Silicalite is also extensively employed for fundamental studies of adsorption in microporous solids (12–15) and for molecular simulation studies because of its energetically homogeneous and well-defined structure.

The separation of a gas mixture by a zeolite is affected by:

1. Size or steric exclusion of certain components of a gas mixture from entering the zeolite pores, whereas the other components enter the pores and are adsorbed.
2. Thermodynamic selectivity, which is a quantitative measure of the preferential adsorption of certain components over others when all components can enter the pores.
3. Kinetic selectivity, which is a quantitative measure of the ability of certain components to enter the pores (and become adsorbed) faster than other components.

Zeolites are called "molecular sieves" because they offer the possibility of gas separation by mode 1. Table 3 compares the size of various adsorbate molecules with the size of pore openings in zeolites. Only a few gas separation processes utilize this mode; the two best examples are gas drying by KA (3A) zeolite and separation of straight and branched chain hydrocarbons by Ca-Na A (5A) zeolite.

Use of mode 3 for kinetic-based gas separation is also rare; the best example is separation of CH_4 and N_2 by NaA (4A) zeolite. High silica, eight-ring zeolites (Si-CHA, ITQ-3, and ZSM-58) have very large differences in propylene and propane sorption rates (16), which suggests a potential for kinetic-based separations of these two gases.

The vast majority of gas separations by zeolites use mode 2. Thermodynamic selectivity for adsorption of a particular gas inside a zeolite cavity is generally made possible by the preferential adsorption of that gas on accessible cationic sites inside the crystal. The adsorption of a gas on the aluminosilicate framework of a zeolite is weak by

Table 3 Examples of Molecules Accepted by Various Zeolites

Zeolite	Approx. window size (Å)	Molecules accepted
KA (3A)	2.8	He, H_2O, NH_3
Ca and Ba mordenite	3.8	Ne, Ar, CO, CO_2, H_2O_2, N_2, O_2, and above
NaA (4A), Na mordenite	4.0	Kr, CH_4, C_2H_6, CH_3OH, CH_3CI, C_2H_2, CS_2, CH_3NH_2, and above
CaA (5A), Ca chabazite	4.9	C_3H_8, n-C_4H_{10}, C_2H_5Cl, C_2H_5OH, $C_2H_5NH_2$, CHF_2Cl CHF_3, CH_3I, B_2H_6, and above
NaX (13X)	7.8	SF_6, i-C_4H_{10}, i-C_5H_{12}, $CHCl_3$, $(CH_3)_2CHOH$, C_3F_8, B_5H_9, CCl_4, $C_2F_2Cl_2$, C_6H_6, $C_6H_5CH_3$, cyclo-C_5H_{12}, cyclo-C_6H_{14}, pyridine, dioxane, naphthalene, quinoline, and above
CaX (10A)	10.0	1,3,5-Triethylbenzene and above

comparison and not very selective. Obviously, the strength and selectivity of adsorption of a gas on a zeolite depends on the size, shape, and structure of the zeolite cavity, cationic charge density, concentrations of cations, polarizability, and permanent polarity of the guest adsorbate molecules. In general, a large or more polar gas molecule will be more strongly and selectively adsorbed on zeolites having smaller pores and a larger cation charge density. Divalent cations generally have larger charge densities than monovalent cations of similar size. Table 4 provides some of the properties of gases relevant to adsorption on zeolites.

High strength and selectivity of adsorption of a particular molecule may be desirable properties for removal of a trace impurity from a gas by TSA processes where external thermal energy is applied to supply the energy of desorption. Such properties are undesirable for bulk gas separation by PSA processes because the desorption is effected under much milder conditions. Selection of an optimal adsorbent based on the ease of desorption is often the key design criterion for bulk gas separations.

Commercial zeolites are generally available in bound forms where the zeolite crystals (1–5 μm) are formed in regular particle shapes (beads, pellets, extrudates, cloverleaf design, etc.) using a binder material (clay, alumina, polymers, etc.). The purpose of the bound forms (diameters of 0.5–6.0 mm are common) is to reduce the pressure drop in adsorbent columns. The binder phase of the bound particles generally contains a network (arteries) of meso- and macropores (0.5–5.0 μm in diameter) to facilitate transport of the adsorbate molecules from the external gas phase to the mouths of the zeolite crystal pores. Pore formers, such as starch or organic chemicals, are often added to the binder and then removed by combustion after the particles are formed. Adsorption of gases on the binder material is generally weak or negligible compared to adsorption on the zeolite. Figure 2 is a schematic drawing of a bound zeolite particle showing the transport path of a gas molecule during the adsorption or desorption process.

Typically, the binder material comprises 10–20% by weight of the pellet mass. Occasionally the binder is converted to a zeolitic structure (the same or different from the original crystals) after the particle formation. The end product in this case is called a "binder-less zeolite," which offers higher specific adsorption capacity.

Table 4 Properties of Selected Adsorbate Gases

Gas	Mol. weight (g/mol)	Critical temp. (K)	Critical pressure (bar)	Critical volume (cm^3/mol)	Normal boiling point (K)	Liquid volume at NBP (cm^3/mol)	Kinetic diameter (Å)	Polariz-ability $\times 10^{-25}$ (cm^3)	Dipole moment $\times 10^{18}$ (esu cm)	Quad. moment $\times 10^{26}$ (esu cm^2)
Ar	39.948	150.9	48.98	74.6	87.3	28.7	3.542	16.41	0.0	0.0
CH_4	16.043	190.6	45.99	98.6	111.7	37.8	3.758	26.00	0.0	0.0
CH_3Cl	50.488	416.3	66.80	143	249.1	50.8	4.182	47.2–53.5	1.87	
CH_2Cl_2	84.932	510	60.8	185	313.0	65.8	4.898	64.8	1.62	
$CHCl_3$	119.377	536.4	54.72	239	334.3	84.6	5.389	82.3	1.01	
CCl_4	153.822	556.4	45.60	276	349.9	103.6	5.947	105.	0.0	
CCl_2F_2	120.914	385.0	41.4	216.7	245.2	79.8		78.1–79.3	0.51	
CF_4	88.005	227.6	37.4	139.6	145.1	53.5	4.7	38.4	0.0	
C_2H_6	30.070	305.3	48.72	145.5	184.5	55.0	4.443	44.70	0.0	0.65
C_2F_6	138.012	293.0	30.6	222	194.9	86.8		68.2	0.0	
C_2H_2	26.038	308.3	61.39	113	192.4[c]	42.7	3.30	33.3	0.0	
C_2H_4	28.054	282.3	50.40	131	169.4	49.4	4.163	42.60	0.0	1.5
C_3H_6	42.081	365.6	46.65	188.4	225.5	69.1	4.678	62.60	0.366	
C_3H_8	44.097	369.8	42.48	200.0	231.1	75.7	4.3–5.12	62.9	0.084	
n-C_4H_{10}	58.123	425.1	37.96	255	272.7	96.6	4.687	82.0	0.05	
i-C_4H_{10}	58.123	408.1	36.48	262.7	261.4	97.8	5.278	82.90	0.132	
1-butene	56.108	420.0	40.43	239.3	266.9	89.6		79.7–85.2	0.34	
2-butene[a]	56.108	428.6	41.00	237.7	274.0	89.6			0.5	
n-C_5H_{12}	72.150	469.7	33.70	313	309.2	118.4	5.784	99.9	0	

n-C_6H_{14}	86.177	507.6	30.25	371	341.9	140.8	5.949	119	0	
n-C_7H_{16}	100.204	540.2	27.40	428	371.6	163.8		137	0	
n-C_8H_{18}	114.231	568.7	24.90	486	398.8	187.5		159	0	
i-C_8H_{18}[b]	114.231	544.0	25.68	468	372.4	184.1			0	
Toluene	92.141	591.8	41.06	316	383.8	118.2		123	0.36	
CO	28.010	132.9	34.99	93.4	81.6	35.5	3.69	19.5	0.112	2.50
CO_2	44.010	304.2	73.83	94.0	216.55[c]	37.4	3.30–3.94	26.50	0.0	4.30
HCI	36.461	324.7	83.1	81	188.1	30.6	3.34	26.3	1.084	3.8
H_2	2.016	33.19	13.13	64.1	20.28	28.5	2.89	8.0	0.0	0.662
He	4.003	5.2	2.28	57.3	4.22	22.4	2.55	2.04	0.0	0.0
H_2O	18.015	647.1	220.55	55.9	373.15	18.8	2.641	14.50	1.87	
H_2S	34.082	373.5	89.63	98.5	213.5	34.3	3.623	37.80	1.0–1.1	
Kr	83.8	209.4	55.02	91.2	119.9	34.6	3.655	24.84	0.0	0.0
Ne	20.18	44.4	27.6	41.6	27.1	16.0	2.82	3.96	0.0	0.0
NF_3	71.002	234.0	45.3	—	144.4	46.2		3.62	0.235	
NH_3	17.031	405.7	112.8	72.5	239.8	25.0	2.900	22.6	1.30–1.47	
N_2	28.014	126.2	34.00	89.2	77.4	34.7	3.64–3.80	17.60	0.0	1.52
N_2O	44.013	309.6	72.45	97.4	184.7	35.9	3.3	29.21	0.167	
O_2	31.999	154.6	50.43	73.4	90.2	27.9	3.467	16.00	0.0	0.39
SF_6	146.054	318.7	37.6	198.8	209.6	77.0	5.128	65.4	0.0	0.0
Xe	131.30	289.7	58.4	118.0	165.0	42.9	4.047		0.0	0.0

[a] trans.
[b] 2,2,4-Trimethylpentane.
[c] Triple Point.

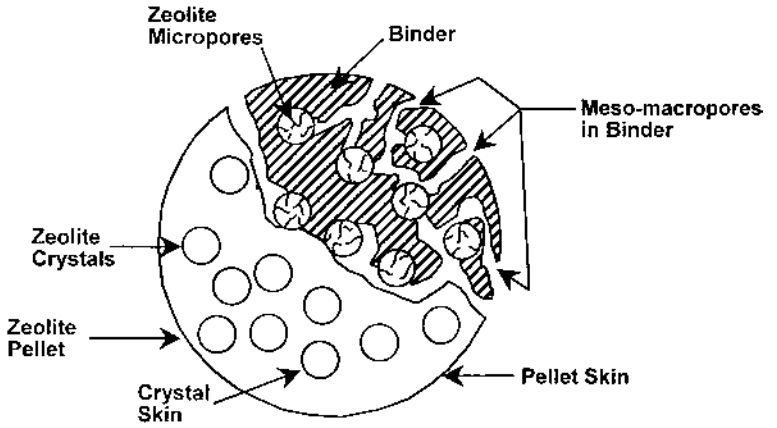

Fig. 2 Structure of a bonded zeolite bead.

II. PROPERTIES OF ZEOLITES FOR GAS SEPARATION

Pure and multicomponent gas adsorption equilibria on zeolites are measured by gravimetric, volumetric, closed-loop recycle, chromatographic, column dynamic, frequency response, and isotope exchange (17–19) techniques. There exists a preponderance of pure component data in the published literature. Binary gas adsorption data in zeolites are less common, and multicomponent (ternary and higher) gas adsorption data are rare. The monograph *Adsorption Equilibrium Data Handbook* by Valenzuela and Myers (20) contains most of the published data up to 1989.

The adsorption isotherm of a pure gas on a microporous zeolitic adsorbent is generally type I by the Brunauer classification (21). The specific amount adsorbed (n) at

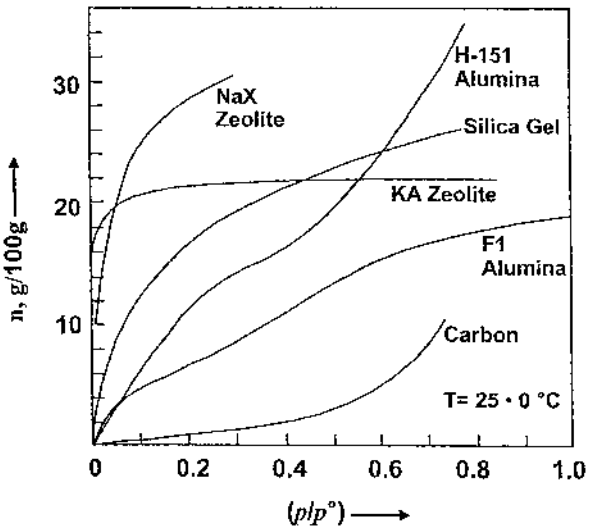

Fig. 3 Adsorption isotherms of water vapor on various adsorbents at 25°C. p/p^0 is relative vapor pressure.

Table 5 Henry's Law Constants for Water Vapor on Various Dessicants at 25°C[a]

Adsorbent	K (g/g)
Carbon (Ceca)	0.056
Alumina F1 (Alcoa)	0.640
Alumina H-151 (Alcoa)	0.900
Silica gel (Grace)	5.5
NaX zeolite (Bayer)	20.0
KA zeolite (Bayer)	> 58.0

[a] Units are grams of water per gram of adsorbent per unit of relative vapor pressure (p/p°).

temperature T increases linearly with pressure (P) at very low pressures. This initial part of the adsorption isotherm where $(\partial n/\partial P)_T = K(T)$ is called the Henry's law region and the slope (K) is called the Henry's law constant. At higher pressure, the slope of the isotherm decreases progressively with increasing gas pressure and finally approaches asymptotically the saturation adsorption capacity (m) of the zeolite. The Henry's law constant K decreases with increasing temperature because adsorption is an exothermic process. At low temperature, it may not be possible to measure K experimentally for a strongly adsorbed gas because the Henry's law region exists only at extremely low pressures. Nevertheless, accurate K values for such systems may be measured at a higher temperature where the Henry's law region extends to higher values of pressure.

Figure 3 shows adsorption isotherms of water vapor on KA (3A) and NaX (13X) zeolites at 25°C and compares them with isotherms for other porous desiccants (22). The amount adsorbed is plotted against the relative vapor pressure (p/p°) of water. Both

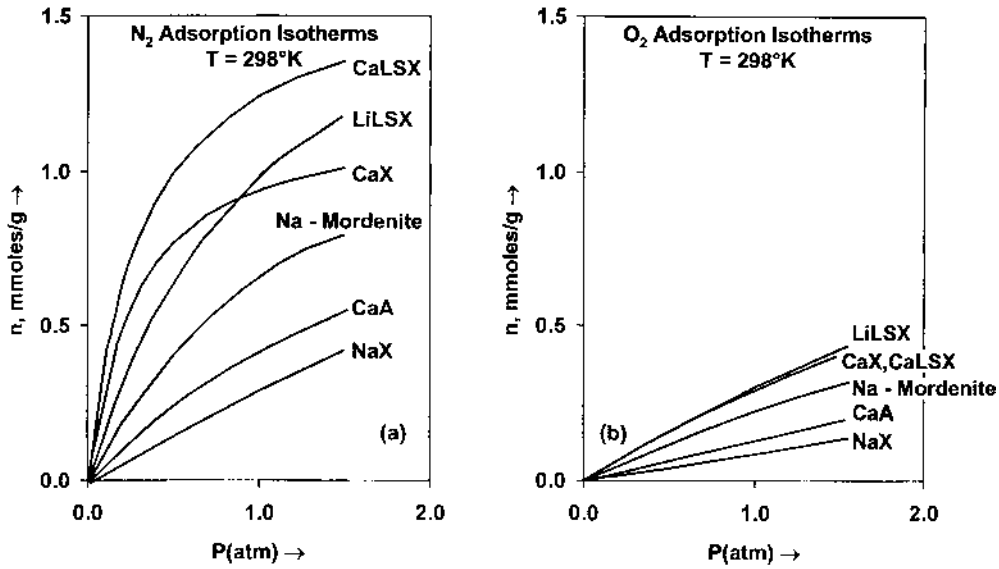

Fig. 4 Adsorption isotherms of (a) nitrogen and (b) oxygen on various zeolites at 25°C.

Table 6 Adsorption Characteristics of N_2 and O_2 on Various Zeolites at 25°C

	N_2			O_2			
Zeolite	m (mol/kg)	K (mol/(kg atm))	$q°$ (kcal/mol)	m (mol/kg)	K (mol/(kg atm))	$q°$ (kca1/mol)	Selectivity $s°$ (K_{N_2}/K_{O_2})
Ca-NaA (5A)	1.41	0.611	5.7	1.41	0.149	3.6	4.1
Na-mordenite	1.47	1.167	6.2	1.47	0.269	4.4	4.3
NaX	3.12	0.334	4.3	3.12	0.092	3.1	3.6
CaX	1.20	4.394	7.1	1.20	0.392	4.2	11.2
Ca-LSX	1.66	4.888	6.9	1.66	0.370	4.3	13.2
Li-LSX	2.05	1.869	4.2	2.05	0.362	3.3	5.2

zeolites exhibit type I isotherm shapes with very large Henry's law constants (Table 5). Silica gel also has a type I isotherm but with a much smaller value of K. The carbon is essentially hydrophobic and the two aluminas exhibit type IV isotherms (21). The very strong adsorption of water on the zeolites is caused by interaction of the permanent and large dipole moment of water with a zeolite cation. The Henry's law constant for adsorption of water on KA zeolite is much larger than that for the NaX zeolite due to the smaller cavity of the A zeolite and the higher charge density of the K ion.

Figure 4a and b shows adsorption isotherms for pure N_2 and O_2, respectively, on various ion-exchanged zeolites at 25°C (23–24). All of the isotherms are Type I but they have very different values of Henry's law constants and saturation capacities (Table 6). The figures show the influence of zeolite crystal structures and the nature of the cations contained in the zeolites. The larger permanent quadrupole of N_2 compared to that of O_2 (Table 4) is responsible for the stronger affinity of N_2 on these zeolites.

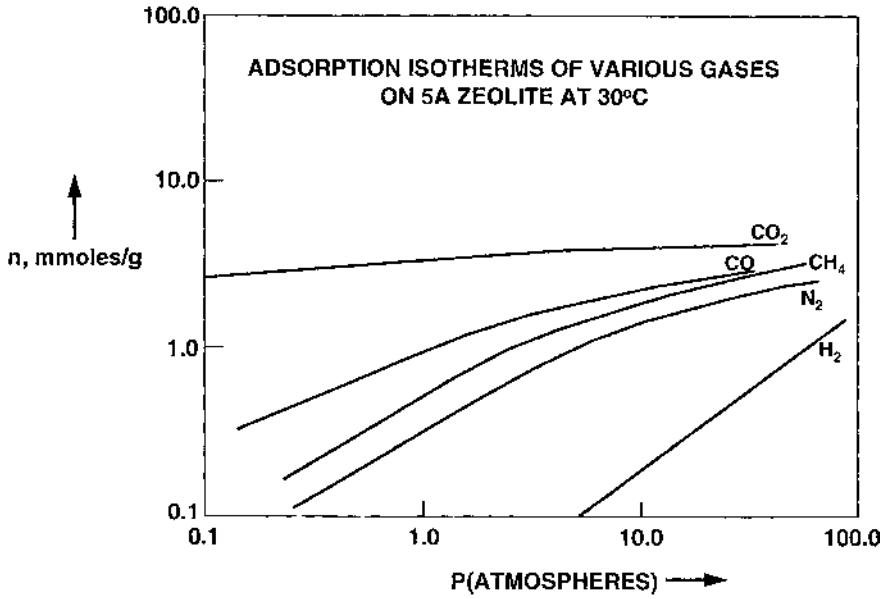

Fig. 5 Adsorption isotherms of various gases on 5A zeolite at 30°C.

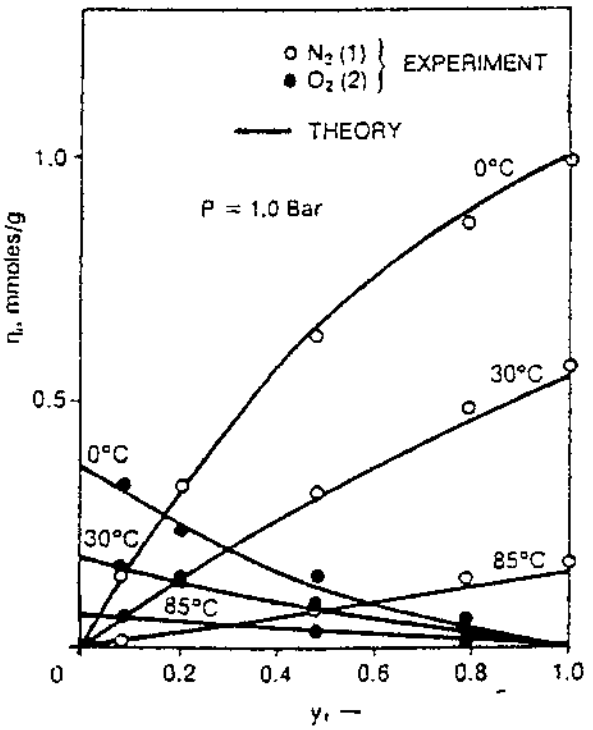

Fig. 6 Adsorption isotherms of binary mixtures of nitrogen and oxygen on Na mordenite at 0°, 30°, and 85°C and 1 bar.

Figure 5 shows a set of isotherms for adsorption of pure CO_2, CO, CH_4, N_2, and H_2 on 5A zeolite at 30°C (25). CO_2 is the most strongly adsorbed gas and H_2 is the most weakly adsorbed gas on 5A zeolite. The strength of adsorption of the three other gases is in the order CO > CH_4 > N_2. The larger polarizability of CH_4 compared to N_2 creates a stronger interaction energy with the the zeolite despite the quadrupole moment of N_2.

Typical characteristics of binary gas adsorption isotherms on zeolites are represented by the example given in Fig. 6, which shows adsorption of binary mixtures of N_2 and O_2 on Na-mordenite at a pressure of 1 atm and 0°, 30°, and 85°C (26). The amounts (n_i) of ith component adsorbed are plotted as functions of its gas phase mole fraction (y_i) at constant pressure and temperature.

III. SELECTIVITY OF ADSORPTION

The binary selectivity for adsorption of component i relative to component j in a multicomponent gas mixture is defined by:

$$s_{ij} = \frac{n_i y_j}{n_j y_i} \tag{1}$$

The selectivity (s_{ij}) decreases with increasing temperatures for a given adsorbate loading (n_i). At constant temperature on an energetically homogeneous zeolite the selectivity can be constant, increase, or decrease with adsorbate loading depending of the relative size of the adsorbate molecules (27). At constant temperature on an energetically heterogeneous

zeolite, the selectivity generally decreases with increasing adsorbate loading (28); thus the maximal selectivity is given by the value in the Henry's law region ($s_{ij}^{\circ} = K_i/K_j$).

The selectivity for a pair of gases on a zeolite depends on the zeolite structure, types and concentrations of cations present in the framework, and accessibility of the cations to the adsorbate gases. Table 6 gives a spectrum of selectivities for adsorption of N_2 and O_2 for different zeolite structures and for different cations in the same zeolite structure. Figure 7a and b shows the pure N_2 adsorption capacity (0.9 atm, 23°C) and selectivity of N_2 over O_2 from air (1.45 atm, 30°) as functions of the degree of Li exchange in a Na-Li-LSX zeolite (29,30). Both properties remain essentially constant until the Li exchange reaches a threshold value, at which point both properties increase rapidly with increasing degree of Li ion exchange. The initial absence of any effect of Li exchange on adsorptive properties is due to the inaccessibility of Li cations by the adsorbate molecules. According to Fig. 7b, the selectivity of N_2 over O_2 from air at 30°C approaches a value of 10 for 100% Li-exchanged LSX zeolite. The value of selectivity given in Table 6 for Li-LSX is much less because the commercial sample may not be completely Li exchanged.

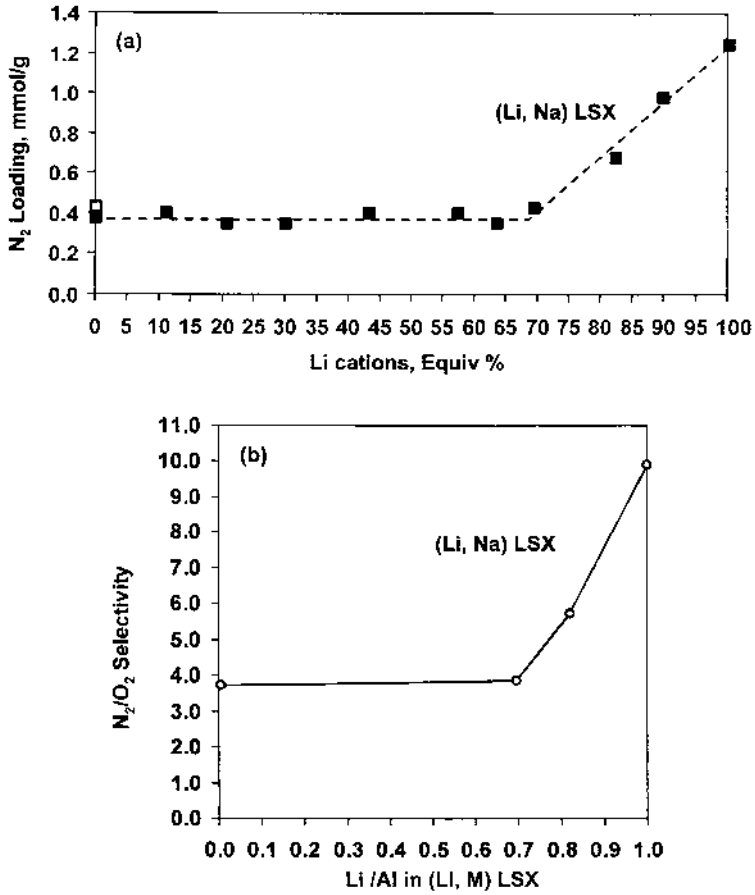

Fig. 7 Effects of the degree of lithium ion exchange in Na-LSX zeolite: (a) nitrogen capacity; (b) nitrogen-oxygen selectivity.

Table 7 Henry's Law Selectivity of Several Binary Gas Mixtures at 303 K

Gas mixture	5A zeolite	BPL carbon
CO_2-CH_4	195.6	2.5
CO_2-CO	59.1	7.5
CO_2-N_2	330.7	11.1
CO_2-H_2	7400.0	90.8
CO-CH_4	3.3	0.33
CO-N_2	5.6	1.48
CO-H_2	125.0	12.1
CH_4-N_2	1.7	4.5
CH_4-H_2	37.8	36.6
N_2-H_2	22.3	8.2

Table 7 gives Henry's law selectivities for various binary gas mixtures at 30°C on 5A zeolite and on BPL carbon, which is a nonpolar, hydrophobic, amorphous adsorbent (25). Gases with larger permanent multipole moments such as CO_2 exhibit much larger selectivities over more weakly polar (CO,N_2) or relatively nonpolar (CH_4,H_2) gases on 5A zeolite compared to the carbon. It is interesting that the preference for adsorption is reversed for the CO/CH_4 binary on the two adsorbents; and the selectivity for CH_4 over N_2 is higher on carbon than on the 5A zeolite.

Adsorption azeotropy, which occurs when the selectivity s_{ij} is equal to unity, has been observed on zeolites (31). Azeotropy is generally associated with intersecting adsorption isotherms as shown in Fig. 8a for adsorption of CO_2 and C_3H_8 on H-mordenite. Figure 8b shows a plot of the binary selectivity s_{CO_2/C_3H_8} as a function of the

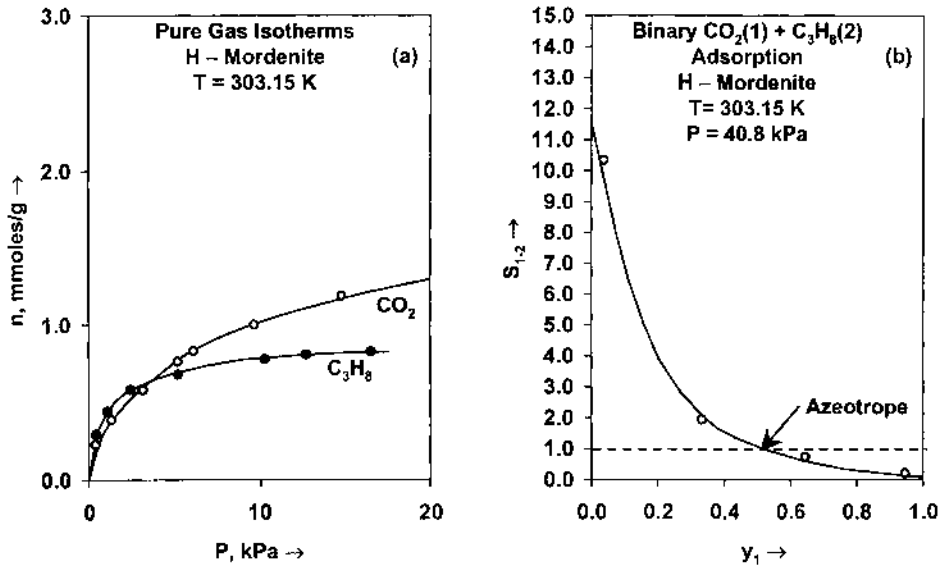

Fig. 8 Adsorption of carbon dioxide and propane on H-mordenite: (a) Pure gas isotherms at 30°C; (b) binary selectivity at 30°C and 40.8 kPa.

mole fraction of CO_2 (y_{CO_2}) at 303.15 K and a total pressure of 40.8 kPa in the gas phase. The modernite is selective for CO_2 over C_3H_8 for $y_{CO_2} < 0.54$, but an azeotrope occurs at $y_{CO_2} = 0.54$ and then the preference for adsorption switches to C_3H_8.

IV. MODELS FOR ADSORPTION EQUILIBRIUM

The classical thermodynamics of adsorption is based on the concept of an inert adsorbent and the introduction of two new variables: surface area and spreading pressure. This approach is standard in adsorption but does not apply to zeolites because neither the surface area nor the spreading pressure has any meaning inside the micropore of a zeolite. Solution thermodynamics is superior to two-dimensional surface thermodynamics for adsorption in zeolites, both in theory and in practical usage (32,33).

Perfect zeolite crystals are physicochemically homogeneous but real, commercial zeolites can be energetically heterogeneous due to lattice defects, variations in the silica/alumina ratio in the framework, presence of hydrated and dehydrated cations at different locations within the framework, nonuniform hydrolysis of the framework during regeneration, and presence of trace amounts of moisture. Heterogeneity can also be introduced by the binder phase in a pelletized zeolite particle. Most models of adsorption equilibrium developed for describing type I isotherms apply to zeolite systems. Table 8a lists several models that give analytical equations for pure and multicomponent adsorption equilibria and are thermodynamically consistent (34). Most of these models have been used to describe adsorption of gases on zeolites.

The thermodynamically consistent ideal adsorbed solution (IAS) theory (35) has also been used to calculate multicomponent gas adsorption on zeolites from pure-gas adsorption isotherms. The conditions under which IAS theory can be successfully employed and methods for estimating corrections have been studied recently (36,37). Other models, such as the Freundlich isotherm (21), loading ratio correlation (38), and the virial equation (13), have also been used to describe gas adsorption on zeolites.

The N_2 and O_2 isotherms for Na-mordenite on Fig. 4 can be fitted satisfactorily by the Langmuir equation (23). The binary adsorption data on Fig. 6 agree with the binary Langmuir equation in Table 8a using constants derived from the pure-gas data (26). The Langmuir equation works in this case because the experimental data in Fig. 4 are in the low-pressure region. For most systems, the two-constant Langmuir equation doesn't fit the single-gas isotherms very well; in such cases, the combination Langmuir-virial equation is recommended for adsorption in zeolites (37).

V. HEATS OF ADSORPTION

The differential enthalpy change for the isothermal transfer of an infinitesimal amount of adsorbate from the adsorbed phase to the gas phase is called the isosteric heat of adsorption (q) (32). Normally adsorption is exothermic and desorption is endothermic.

The isosteric heat of a pure gas (q_i°) and the isosteric heats for the components of a gas mixture (q_i) can be measured directly as functions of absorbate loadings (n_i^0 or n_i) and temperature using a microcalorimeter (39–44). However, published calorimetric data are sporadic. Multicomponent (ternary and higher) heat data are rare. Most published data on isosteric heats of adsorption of pure gases are obtained from adsorption isotherms at different temperatures using thermodynamic relations (19). A plot of $\ln(P)$ against reciprocal absolute temperature ($1/T$) at constant adsorbate loading (n) has a slope equal to $(-q^\circ/R)$, where R is the gas constant. Slopes taken at different loadings give the isosteric

Table 8a Equations for Pure and Multicomponent Gas Adsorption Isotherms on Zeolites

Model	Requirement	Pure gas	Multicomponent gas	Thermodynamic constraint
Langmuir	Homogeneous zeolite, equal-sized adsorbates	$b_iP = \frac{\theta_i^0}{(1-\theta_i^0)}$	$b_iPy_i = \frac{\theta_i}{(1-\Sigma\theta_i)}$	$m_i = m_j = \text{constant}$
Multisite Langmuir	Homogeneous zeolite, unequal-sized adsorbates,	$b_iP = \frac{\theta_i^0}{(1-\theta_i^0)^{a_i}}$	$b_iPy_i = \frac{\theta_i}{(1-\Sigma\theta_i)^{a_i}}$	$m_ia_i = \text{constant}$
Martinez-Basmadjian	Homogeneous zeolite, unequal-sized adsorbates, lateral interactions	$b_iP = \frac{\theta_i^0}{(1-\theta_i^0)^{a_i}} e^{\frac{-a_i w_{ii}\theta_i^0}{RT}}$	$b_iPy_i = \frac{\theta_i}{(1-\Sigma\theta_i)^{a_i}} e^{-\frac{\Sigma a_i w_{ij}\theta_i}{RT}}$	$m_ia_i = \text{constant}$, $w_{ij} = 0$
Toth	Heterogeneous zeolite, equal-sized adsorbates	$b_iP = \frac{\theta_i^0}{[1-(\theta_i^0)^k]^{1/k}}$	$b_iPy_i = \frac{\theta_i}{[1-(\Sigma\theta_i)^k]^{1/k}}$	$m_i = m_j = \text{constant}$

Notes:
$\theta_i^0 = (n_i^0/m_i)$ = fractional coverage of pure gas i
$\theta_i = (n_i/m_i)$ = fractional coverage of ith gas in mixture
n_i = specific amount adsorbed of ith component (mol/kg)
m_i = saturation capacity of ith component (mol/kg)
$b_i = b_i^0 e^{q_i^*/RT}$ = gas–solid interaction parameter of ith gas (bar^{-1})
b_i^0 = constant for pure gas i (bar^{-1})
a_i = number of adsorption sites per molecule of i
w_{ii} = lateral interaction parameter (J/mol) for component i
k = heterogeneity parameter for all adsorbates
q_i^* = limiting value of isosteric heat of pure i (J/mol) in Henry's law region

Table 8b Equations for Isosteric Heat of Adsorption on Zeolites

Model	Pure gas	Multicomponent gas
Langmuir	$q_i^0 = q_i^* = \text{constant}$	$q_i = q_i^0$
Multisite Langmuir	$q_i^0 = q_i^* = \text{constant}$	$q_i = q_i^0$
Martinez-Basmadjian	$q_i^0 = q_i^* + a_i w_{ii} \theta_i$	$q_i = q_i^* + \Sigma_j a_i w_{ij} \theta_j$
Toth	$q_i^0 = q_i^* + \frac{RT^2}{k} \frac{d\ln k}{dT} F(\theta_i^0)$	$q_i = q_i^* + \frac{RT^2}{k} \frac{d\ln k}{dT} F(\theta)$

Notes:
$F(x) = \frac{(1-x^k)\ln(1-x^k)+x^k\ln(x^k)}{(1-x^k)}$ *where* $x = \theta_i^0$ *or* θ

$\theta = \Sigma_i \theta_i$

heat as a function of loading, as illustrated in Fig. 9 for adsorption of pure CO_2 on NaX zeolite crystals (45).

A useful and frequently used approximation is that the isosteric heat is independent of temperature, at least over some modest interval of temperature. Figure 10a and b shows a test of this assumption for the isosteric heat of adsorption of CO_2 on a pelletized sample of silicalite and for the isosteric heat of adsorption of N_2 on a pelletized sample of 5A zeolite (44).

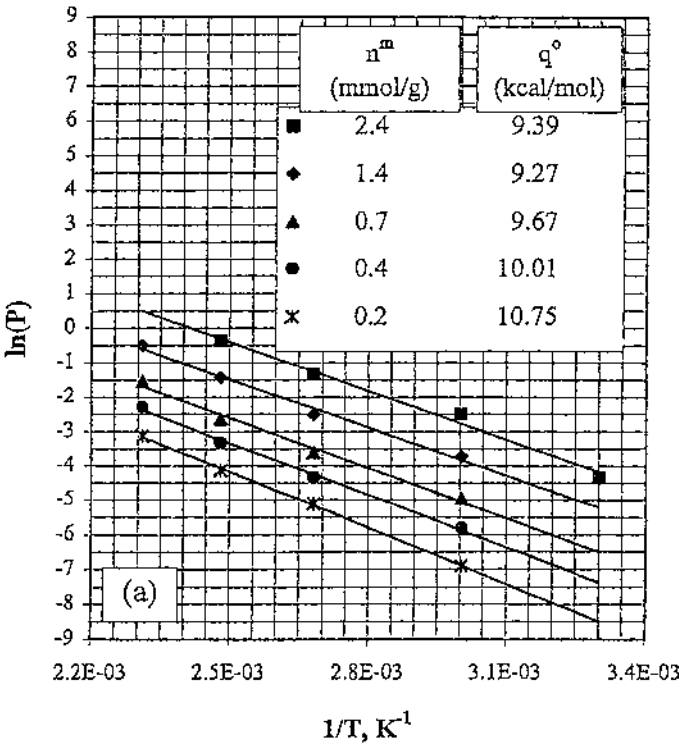

Fig. 9 Plots of ln P vs. $(1/T)$ for adsorption of carbon dioxide on NaX zeolite.

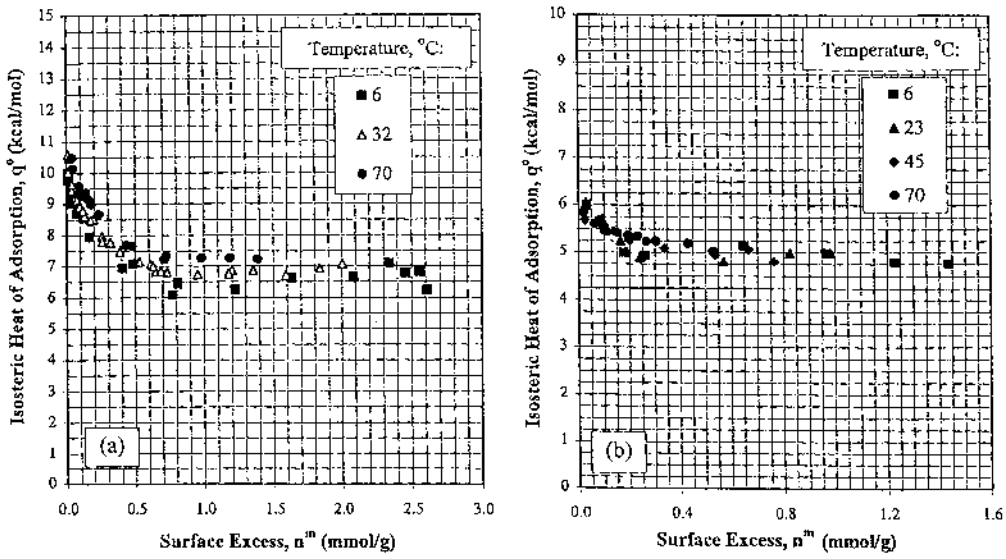

Fig. 10 Isosteric heats of adsorption at different temperatures: (a) carbon dioxide on a bonded silicalite sample; (b) nitrogen on 5A zeolite.

A zeolite is energetically homogeneous to adsorption if its isosteric heat is independent of adsorbate loadings as shown by Fig. 11a (C_2H_6 on silicalite crystals) (39). The zeolite is energetically heterogeneous to adsorption of a gas when the isosteric heat decreases with increasing adsorbate loadings as shown in Figs. 9, 10a and b. Lateral interactions between adsorbed molecules are pronounced if the isosteric heat of a gas increases with adsorbate loadings at higher coverages as shown by Fig. 11b (SF_6 on

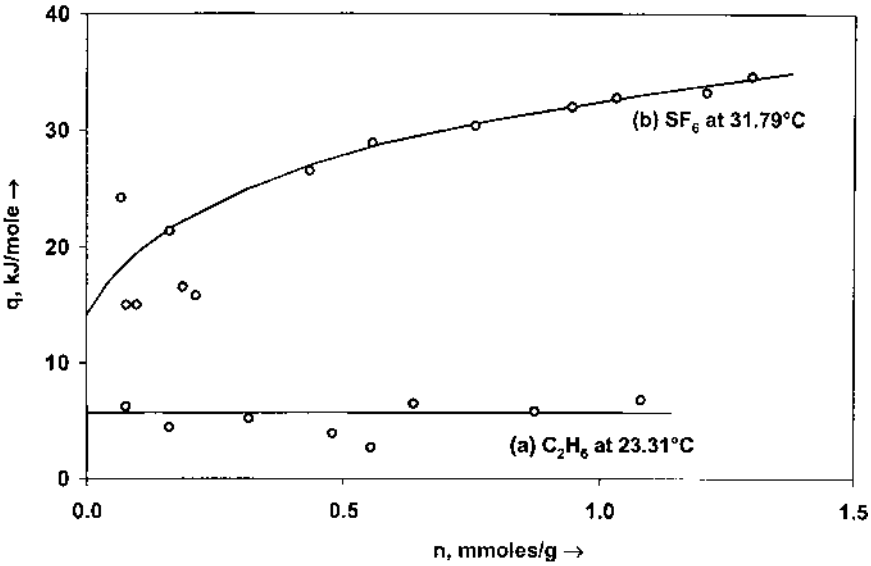

Fig. 11 Isosteric heats of adsorption: (a) ethane on silicalite; (b) sulfur hexafluoride on silicalite.

Table 9 Henry's Law Isosteric Heat of Adsorption at 25°C (kcal/mol)

Gas	Silicalite	NaX	CaX	LiX	5A	Na-mordenite
H_2	1.4				2.2	
N_2	4.2	4.7	7.1	4.2	5.7	6.2
O_2	3.9	3.6	4.2	3.3	3.6	4.4
Ar	3.8	3.0		2.9	3.3	4.8
Kr	3.8	4.4			4.3	
CH_4	5.0	4.6			5.1	
C_2H_6	7.4	6.5			5.9	
C_3H_8	9.8				8.4	
n-C_4H_{10}	12.1				10.4	
CO_2	6.5	11.7			9.5	
CO	4.0	5.5			8.3	
SF_6	8.2	6.7				
H_2O		18.0			18.0	

silicalite crystals) (39). The effects of zeolite heterogenity and lateral interactions may counterbalance each other resulting in a constant (or slowly changing with adsorbate loading) isosteric heat of adsorption.

The limiting isosteric heat of adsorption of a pure gas in the Henry's law region (q_i^*) is often treated as the characteristic interaction energy between the gas and the zeolite. (q_i^*) increases with the polarizability and polarity (see Table 4) of the adsorbate molecule. Table 9 gives typical examples of limiting isosteric heats on various zeolites, but published values exhibit significant variations.

Isosteric heats of adsorption of the components of a gas mixture on a zeolite (q_i°) are complex functions of adsorbate loadings unless the zeolite is energetically homogeneous to all components. Figure 12a and b shows calorimetrically measured isosteric heats of CO_2 and C_2H_6 from their mixtures on NaX zeolite at 29°C as functions of CO_2 loading at constant loadings of C_2H_6 (41).

A. Models for Isosteric Heats

Analytical equations describing isosteric heats of adsorption of pure and multicomponent gases as functions of adsorbate loading can be derived by applying thermodynamics to analytical adsorption equilibrium models (33). Table 8b provides expressions for isosteric heats of adsorption corresponding to various type 1 equilibrium models. The isosteric heat of adsorption (q_i) of component i is equal to that for the pure gas (q_i^0) on a homogeneous zeolite. Otherwise q_i differs from q_i^0, even at the same loading.

Isosteric heats are needed for heat balance equations in process design of adsorber columns (46), so analytical equations for these variables are extremely useful.

VI. ADSORPTION KINETICS

The rates of adsorption and desorption of a gas for a particular site inside a zeolite crystal are extremely rapid, of the order of microseconds. However, the transport of a gas molecule from the gas phase outside a bound zeolite particle to an adsorption site (see Fig. 2) is slowed by the existence of several series and parallel transport resistances along

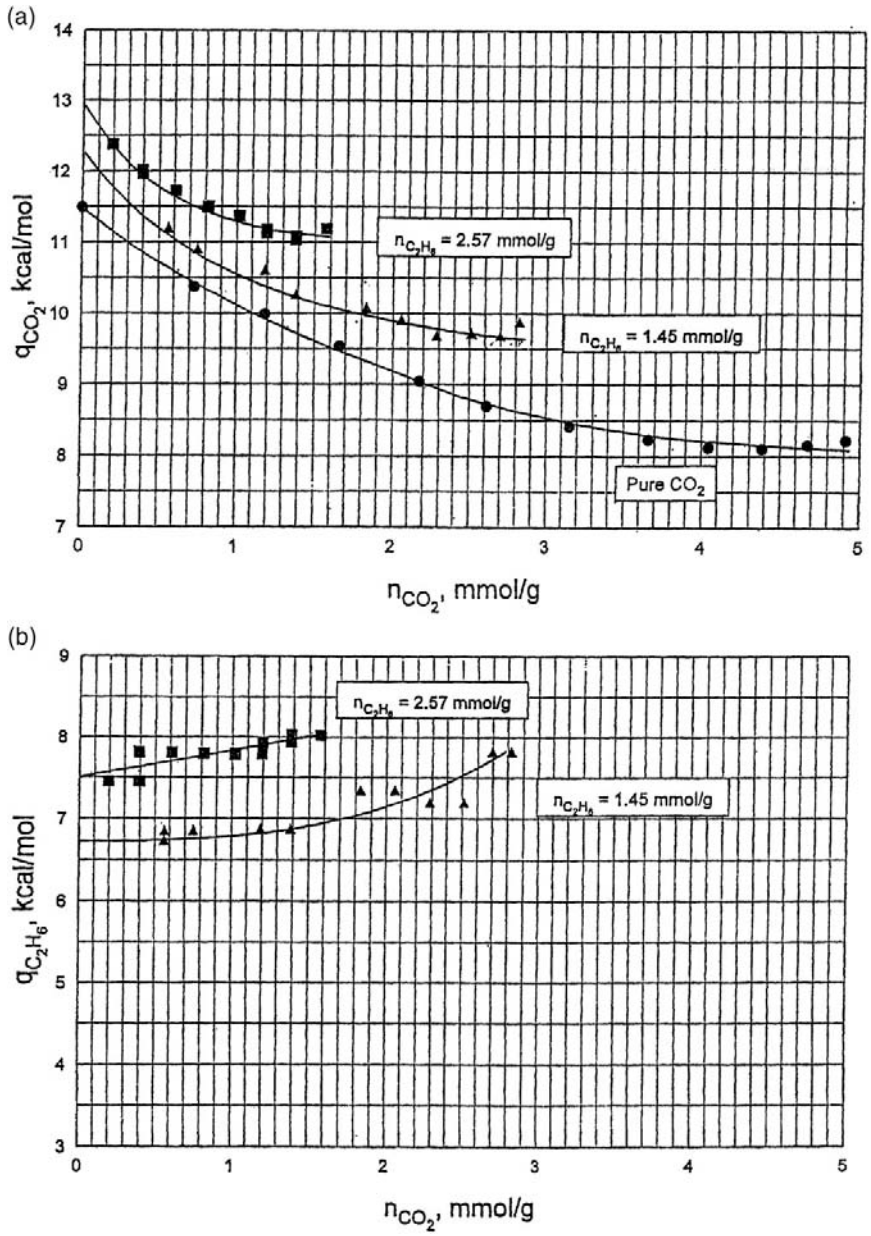

Fig. 12 Isosteric heats of adsorption of carbon dioxide and ethane binary gas mixtures on NaX zeolite: (a) carbon dioxide; (b) ethane.

the path. The description of this transport process is referred to as *adsorption kinetics* in the literature. The following transport resistances are recognized:

1. *External gas film resistance outside the adsorbate particle (for mixtures only)*. The mechanism for this transport is gas–gas diffusion.
2. *Diffusional resistances through the network of pores within the binder phase to the surface of the zeolite crystals*. Simultaneous viscous and Knudsen diffusion through the binder pores as well as surface diffusion of molecules adsorbed on the pore walls are mechanisms for this transport mode.
3. *Diffusional resistances through the micropores of the zeolite crystals to the adsorption sites*. The transport mechanism is activated diffusion (hopping) of adsorbed molecules from site to site.

In addition, skin resistances at the surface of the adsorbent particle or at the surface of the crystal have been observed (26,47). Skin resistance is created by the formation of a thin but denser layer of material at the surface during the extrusion of the pellet and by surface hydrolysis during thermal regeneration processes.

Most of the methods for measurement of adsorption equilibria mentioned earlier can be utilized to measure adsorption kinetics. However, most of these procedures (an exception is the frequency response technique) are capable of following only relatively slow adsorption kinetics. Most techniques measure the *transport* diffusivity driven by the gradient of the chemical potential of an adsorbate between the gas and adsorbed phases. The data analysis is model dependent and complicated by the nonisothermal nature of the process. Other methods such as isotope exchange, nuclear magnetic resonance–pulsed field gradient (NMR-PFG), and neutron diffraction (18,48–50) measure the *self-diffusivity* of the adsorbate molecules within the zeolite crystals and particles under isothermal conditions in the absence of a chemical-potential gradient.

Much work has been done to correlate self (D) and transport (D_T) diffusivities for zeolites (18,51). It is generally accepted that these two properties are equal in the Henry's law region (18,51), and that the Darken correction (see Table 12) provides the relationship between the two properties to first order (18). For pure-gas adsorption, $D_T = D[d \ln P/d \ln n]_T$, where $n(P)$ is the adsorption isotherm at T. The relationships become more complicated for mixtures (18,51).

As is the case for equilibrium data, a large volume of kinetic data for adsorption of pure gases on zeolites is available in the published literature. Kinetic data on binary systems are sporadic and kinetic data for multicomponent (ternary and higher) systems are rare. The monograph *Diffusion in Zeolites and Other Microporous Solids* by Karger and Ruthven (18) contains a useful compilation of data. It should be noted that zeolite diffusivities measured by different techniques and laboratories often differ by several orders of magnitude; probable causes cited are differences in sample preparation, heat effects, presence of impurities, and different degrees of hydration.

The diffusion of gases through the micropores of a zeolite framework is generally described by the the Fickian diffusion model (see Table 12). Figure 13a shows an example for kinetics of adsorption of pure N_2, CH_4, and Kr on a pelletized sample of 4A zeolite at 283 K (50). The data were measured isothermally using the isotope exchange technique. Figure 13b shows the dependence of Fickian self-diffusivities of these gases on fraction of the equilibrium amount adsorbed (θ). The variable D_i^{*0} is the self-diffusivity for adsorbate i at the limit of zero coverage given by Table 10, which also shows the Henry's law constants, limiting isosteric heats, saturation capacities, and activation energies for intracrystalline diffusion for these gases. These data show that despite the remarkable similarities in physical properties of these gases (Table 4) and

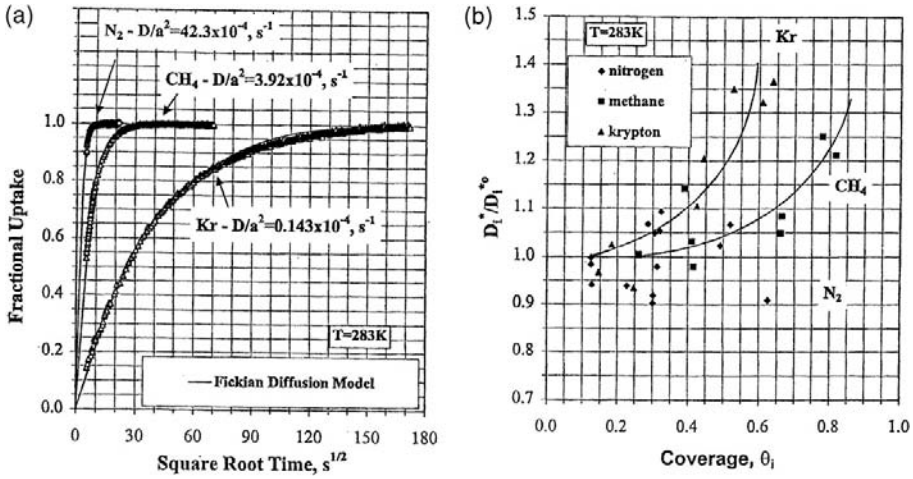

Fig. 13 Kinetics of adsorption of nitrogen, methane, and krypton on 4A zeolite at 10°C: (a) fractional uptake curves; (b) self-diffusivities as functions of adsorbate loading.

their isosteric heats, the diffusivity of Kr in 4A zeolite is an order of magnitude smaller than that for CH_4, and the diffusivity of CH_4 is an order of magnitude smaller than that for N_2. The activation energies for transport within the zeolite pores also differ substantially. Figure 13 shows that the self-diffusivity of N_2 is practically independent of adsorbate loading but the self-diffusivities for CH_4 and Kr increase with loading. The effect is most pronounced for Kr. These complex behaviors are caused by the near equality of the molecular diameter and the pore aperture of the zeolite. It is interesting that the kinetics for binary mixtures of N_2 and CH_4 on 4A zeolite are also Fickian, and the self-diffusivity at a given loading (θ_i) of component i is approximately equal to the self-diffusivity of the pure gas at the same loading ($\theta_i^0 = \theta_i$). Thus, the rate of diffusion of either component is unaffected by the presence of the other component (49).

Figure 14 shows self-diffusivities as functions of adsorbate loadings for adsorption of CH_4, C_2H_6, and C_3H_8 in 5A, silicalite, and NaX zeolites (52). These were measured by the NMR-PFG technique. In this case, the diffusivities decrease with increasing adsorbate surface coverages on NaX and silicalite samples but increase with adsorbate surface coverage on 5A zeolite. Other peculiar behaviors have also been measured (53).

Binary adsorption kinetics on zeolites is a challenging and interesting subject. Figure 15 shows uptakes of CH_4 and N_2 by 4A zeolite from a binary mixture containing 50.9% N_2 and 49.1% CH_4 at atmospheric pressure and 194.1 K. Volumetric

Table 10 Henry's Law Self-Diffusivity of Gases on 4A Zeolite at 283 K

Gas	Kinetic diameter (Å)	Henry's law constant (mol/(kg atm))	Henry's law heat (kcal/mol)	Saturation capacity (mol/kg)	Self-diffusivity (cm^2/s)	Activation energy (kcal/mol)
N_2	3.68	0.52	4.7	2.05	$42.78 \cdot 10^{-4}$	5.24
CH_4	3.82	0.96	4.2	2.42	$3.61 \cdot 10^{-4}$	6.37
Kr	3.49	0.42	4.3	2.61	$0.13 \cdot 10^{-4}$	7.72

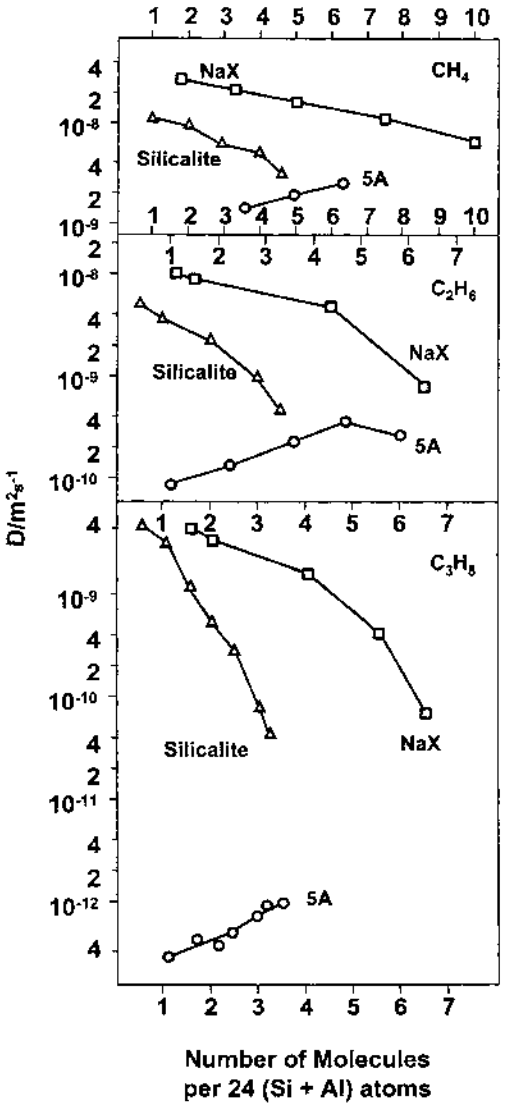

Fig. 14 Self-diffusivities of methane, ethane, and propane as functions of adsorbate loadings on various zeolites at 300 K.

measurements (54) indicate that N_2 adsorbs much faster than CH_4 (Table 10). Since CH_4 is preferentially adsorbed compared to N_2, CH_4 molecules eventually diffuse into the zeolite pores and displace the adsorbed N_2. Thus, the amount of N_2 adsorbed as a function of time (t) passes through a maximum. The data of Fig. 15 show that N_2 can be separated from CH_4 on the basis of its kinetic selectivity even though CH_4 is preferentially adsorbed at equilibrium. A very high value of the kinetic selectivity of 4A zeolite for N_2 can be achieved by using a short contact time in a cyclic PSA process. 4A zeolite (either pure Na form or partially exchanged with K) can also be used to separate air by exploiting its kinetic selectivity for O_2 over N_2 at reduced temperature (55).

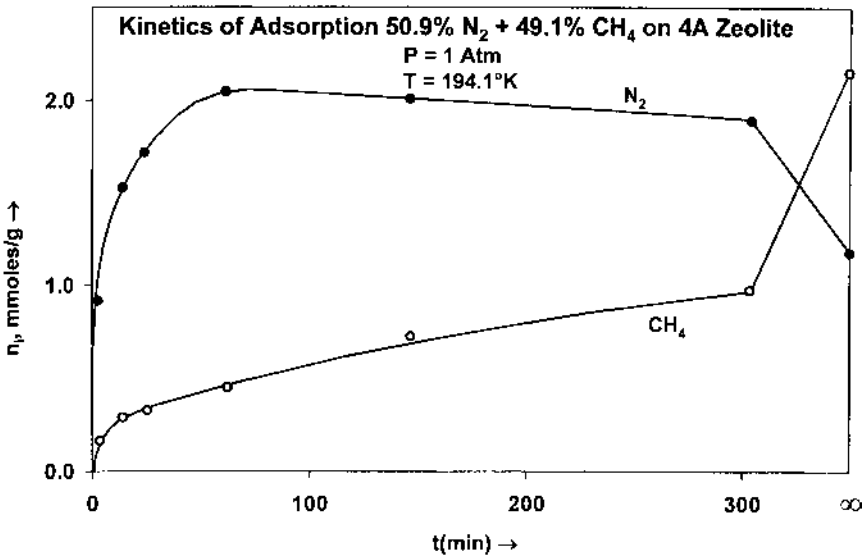

Fig. 15 Kinetics of adsorption of nitrogen-methane binary gas mixture on 4A zeolite at 194 K and 1 atm.

Table 11 is a compilation of Henry's law diffusivities or self-diffusivities (D) of various gases in several zeolites at 300 K. Some of the values were estimated from data measured at other temperatures using the Arrhenius relationship ($D = D_\circ^\circ \exp[-E/RT]$) and the activation energy for intracrystalline zeolite diffusion (E) listed in the table. The striking effect of the relative sizes of the adsorbate molecule and the zeolite pore aperture on the intracrystalline diffusivity is apparent from the data, especially for n-C_4H_{10}.

The characteristic distances for gas diffusion in the zeolite crystal and in the binder phase are given by the crystal radius ($R_c \approx 1$ μm) and the bound particle radius ($R_p \approx 1$ mm), respectively. Thus, the diffusional time constants for the crystals ($\tau_c = D_c/R_c^2$) is generally much larger than that for the binder ($\tau_p = D_p/R_p^2$) even though the intracrystalline diffusivity ($D_c \approx 10^{-8}$–10^{-14} m^2/s) is typically much smaller than the intrapellet

Table 11 Henry's Law Diffusivity (D) and Activation Energy (E) of Gases at 300 K

	NaA (4A)		Na-CaA (5A)		NaX (13X)		Silicalite	
Gas	D (m^2/s)	E (kcal/mol)	D (m^2/s)	E (kcal/mol)	D (m^2/s)	E (kcal/mol)	D (m^2/s)	E (kcal/mol)
O_2	$3.4 \cdot 10^{-12}$	4.54						
N_2	$3.1 \cdot 10^{-14}$	5.73	$1.1 \cdot 10^{-10}$	2.27				
Ar	$7.8 \cdot 10^{-15}$	5.73						
Kr	$1.2 \cdot 10^{-17}$	8.12						
CH_4	$1.2 \cdot 10^{-15}$	5.97	$6.0 \cdot 10^{-10}$				$5.9 \cdot 10^{-9}$	0.96
C_2H_6	$8.0 \cdot 10^{-17}$	5.26	$9.7 \cdot 10^{-11}$	1.44			$4.1 \cdot 10^{-9}$	1.19
n-C_4H_{10}	$9.6 \cdot 10^{-20}$	9.56	$1.5 \cdot 10^{-13}$	4.06	$2.4 \cdot 10^{-11}$	1.43	$6.3 \cdot 10^{-12}$	3.27
CO_2	$8.1 \cdot 10^{-16}$	4.78						
H_2O	$1.4 \cdot 10^{-9}$	1.38			$2.0 \cdot 10^{-8}$		$4.0 \cdot 10^{-9}$	

diffusivity ($D_p \approx 10^{-6}$–10^{-8} m^2/s) for small gas molecules. An exception is adsorption on 4A zeolite where the intracrystalline diffusivity may be controlling. For most cases of adsorption of small molecules on 5A and NaX zeolites, the mesopore-macropore diffusion in pellets constitutes the controlling resistance. However, it is adviseable to confirm this behavior for each application.

A. Models for Adsorption Kinetics

The Fickian diffusion (FD) model is generally used to describe the batch uptake of an adsorbate on a zeolite crystal or a zeolite pellet. A large volume of published work has been analyzed for the kinetics of gas adsorption on zeolites by an isothermal or non-isothermal FD model (17,18). Table 12 summarizes the mathematical FD model and its solution for the simple case of isothermal adsorption on a spherical particle or crystal from a gas phase maintained at constant pressure. Solutions for many other conditions of adsorption are also available.

The FD model is generally deemed mathematically complex for process design and the linear driving force (LDF) model for adsorption kinetics is frequently used to design gas separation processes using zeolites. The isothermal and nonisothermal LDF model has been used to describe batch uptake on zeolites (56). Table 12 summarizes the formalism of the LDF model. Simple correlations between the Fickian diffusivity (D) and the mass transfer coefficient for the LDF model (k) are frequently used for process design (17,57).

Table 12 Models of Isothermal Kinetics for Adsorption of Pure Gases on Zeolites

Model	Mass balance equation	Uptake at constant pressure
Fickian diffusion (FD) on a spherical particle or crystal of radius R	$\left[\frac{\partial c(r,t)}{\partial t}\right]_r = \frac{\partial}{\partial r}\left[\frac{\partial}{\partial r}\left\{r^2 D\left(\frac{\partial c}{\partial r}\right)_t\right\}\right]_t$	
	$\overline{c}\,(t) = \frac{3}{R^3}\int_o^R r^2 c(r,t)dr$	$f(t) = 1 - \sum_{n=1}^{\infty} \frac{6}{(n\pi)^2} e^{-D(n\pi)^2 t/R^2}$
	$D = D_o\left[\frac{d\ln P}{d\ln c}\right]_T$ (Darken correction)	
Linear driving force (LDF) on a spherical particle or crystal of radius R	$\frac{d\overline{c}(t)}{dt} = k[\overline{c}^*(t) - \overline{c}(t)]$	$f(t) = 1 - e^{-kt}$
	$k = \frac{15D}{R^2}$	

Notes:
$c(r,t)$ = adsorbate concentration (mol/m^3) at radius r and time t
$\overline{c}(t)$ = average adsorbate concentration (mol/m^3) in particle
R = radius of particle
D = Fickian diffusivity (m^2/s)
D_o = Diffusivity in Henry's law region or self-diffusivity (m^2/s)
k = LDF mass transfer coefficient (s^{-1})
$f(t)$ = fractional uptake at time t

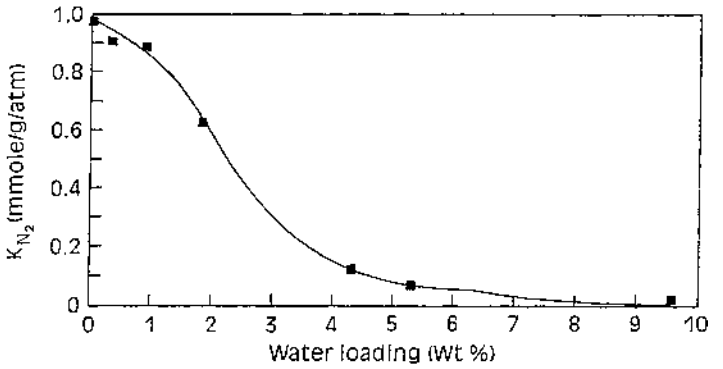

Fig. 16 Henry's law constants for adsorption of nitrogen on Na-mordenite at 30°C as functions of water loadings on the zeolite.

B. Influence of Trace Moisture on Adsorptive Properties

Water is very strongly adsorbed (see Table 9) on most hydrophilic zeolites (except silicalite). Even an extremely dilute amount of preadsorbed water can substantially decrease the adsorption capacity for other gases on zeolites and lower their intracrystalline diffusivity. Figure 16 shows an example of the reduction in the Henry's law constant for adsorption of N_2 at 30°C on Na-mordenite caused by the presence of preadsorbed water (23). The effect of pre-adsorbed water on N_2 and O_2 adsorption on other zeolites has also been reported (58,59).

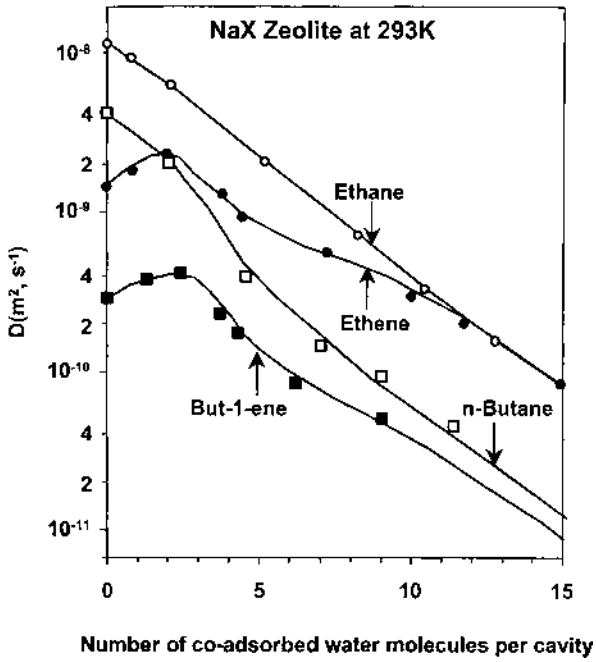

Fig. 17 Self-diffusivities of ethane, ethene, *n*-butane, and but-1-ene on NaX zeolite at 293 K as functions of water loadings on the zeolite.

Figure 17 shows an example of the reduction in the intracrystalline self-diffusivity of C_2H_6, C_2H_4, n-C_4H_{10}, and 1-butene on NaX zeolite at 293 K due to preadsorbed water (53). These data clearly demonstrate the need for regeneration and dehydration of zeolites before their use for gas separations. In fact, most gas separation processes using zeolites require water removal from the feed gas mixture before carrying out the separation of interest.

VII. INDUSTRIAL GAS SEPARATIONS BY ZEOLITES

Numerous practical uses of zeolites for gas separation and purification are listed in Table 1. The following six applications have received the most attention from the R&D and commercial sectors:

1. Gas drying
2. Production of oxygen from air
3. Simultaneous production of nitrogen and oxygen from air
4. Production of hydrogen from steam-methane reformer (SMR) off-gas
5. Simultaneous production of methane and carbon dioxide from landfill gas
6. Separation of normal and isoparaffins

Each of these applications has generated a large volume of scientific, patent, and trade literature covering the use of many different varieties of zeolites and separation process designs (PSA and TSA). During the last four decades, these activities have progressively reduced the unit product cost and energy of separation while improving the purity and recovery of the product gas. A tremendous increase in the scale of production (plant size) has also occurred during this period.

A. Gas Drying

Zeolites type A (3A, 4A, and 5A), type X (Na), mordenite (Na), and chabazite (Na, Ca) have all been used for gas drying by TSA. Zeolites type A (4A and 5A) and type X (Na) are also used for gas drying by PSA.

The basic steps of a TSA gas drying process using zeolites are:

1. Flowing the wet gas over a packed bed of the zeolite at near-ambient temperature and withdrawing a dry product gas
2. Heating the zeolite by the countercurrent flow of a hot, dry gas through the bed while rejecting the water-laden effluent gas
3. Cooling the bed by countercurrent flow of a dry gas through the bed at feed temperature. The effluent gas from this step is rejected or used in step 2 after reheating

A portion of the dry product gas from step 1 is often used as the regenerating gas for steps 2 and 3. The cycle is then repeated. Intermediate steps such as countercurrent depressurization after step 1 and countercurrent pressurization with a dry gas after step 3 are also used when the feed gas is above ambient pressure (22).

Figure 18 is a schematic diagram of a three-bed TSA gas-drying unit. Each adsorber undergoes each step of the process cycle consecutively. The effluent gas from the cooling adsorber (step 3) is heated to provide the hot gas to the regenerating adsorber (step 2). This saves energy by recovering the sensible heat from an adsorber that has just completed step 2. The total cycle time for all three steps for a zeolitic TSA drying process is typically in the range 2–16 h. Typical regeneration temperatures lie in the range 150–350°C. About 10% of dry product gas is used for regeneration. A typical dynamic water removal capacity is 10–20% by weight of the zeolite. Many different regeneration options have

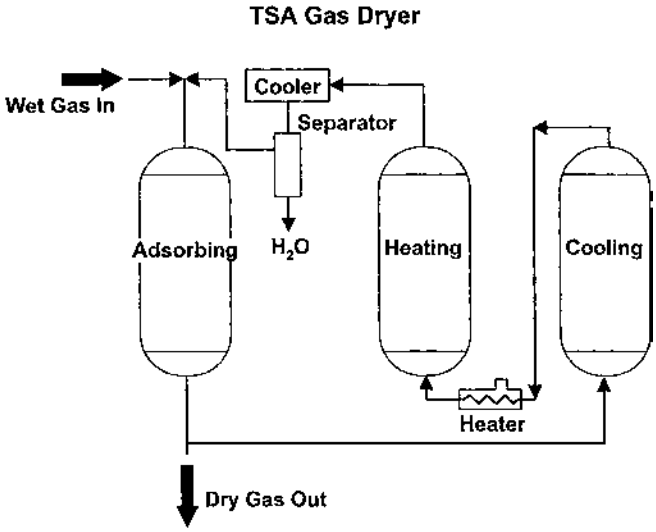

Fig. 18 Schematic diagram of a three-bed TSA dryer.

been developed for decreasing the energy of drying, reducing the adsorbent inventory, and increasing the recovery of dry product gas (22).

Figure 19 shows a typical water breakthrough curve and operating conditions for a 4A zeolite column of length L_0 for drying N_2 (60). The ratio of the gas moisture concentration at the exit of the column (y) to that of the feed gas (y_0) is plotted as a function of elapsed time (t). The mass transfer zone (MTZ) for water adsorption is sharp: the water concentration changes from 1 to 1490 ppm in a relatively short period of time.

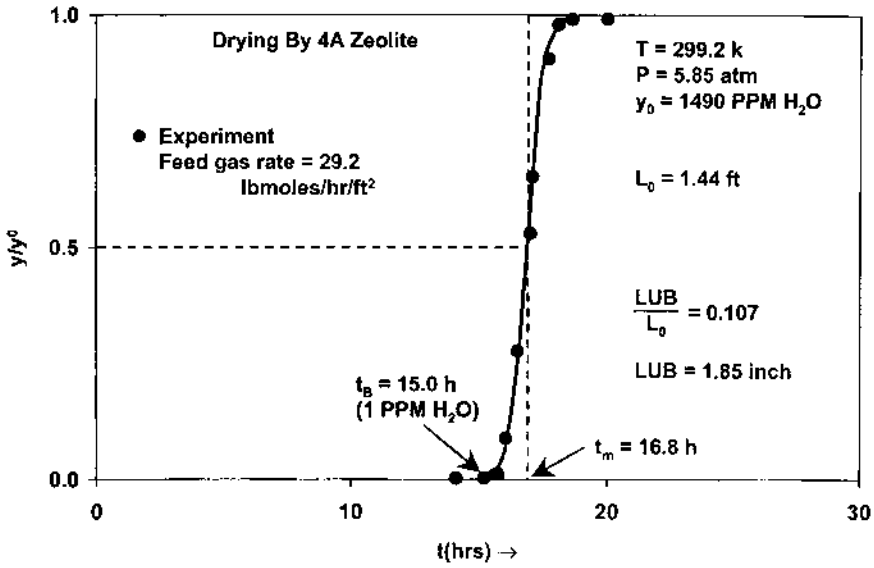

Fig. 19 Column breakthrough curve for adsorption of trace amounts of water from nitrogen gas on 4A zeolite at 299.2 K and 5.85 atm.

The length of the unused bed (LUB) for the system is only 4.7 cm. The LUB is a measure of the dynamic inefficiency of the adsorber. The smaller the value of LUB, the larger the utilization of adsorption capacity of the bed (60). The variable LUB is defined by LUB $= (1 - t_b/t_m)L_0$, where t_b and t_m are the initial impurity break time ($y = 1$ ppm) and stoichiometric break time (no mass transfer resistance for water adsorption). The LUB concept is frequently used for the design of TSA dryers and other TSA trace impurity removal applications using zeolites (60). The very small LUB values for water adsorption at moderate to high feed gas flow rate, coupled with the very large adsorption capacities of zeolites at low partial pressures of water compared to other desiccants (see Fig. 3) make zeolites the preferred candidates for gas drying by TSA (61).

When the concentration of moisture in the feed gas is low ($y^0 \ll 1$), the temperature front developed by the exothermic heat of adsorption of water moves ahead of the water MTZ as shown in Fig. 20 for adsorption of trace water from air by NaA zeolite at 26.7°C (61). This behavior is called type 2 adsorption column dynamics, which is favored when $(n^0/y^0) > (C_g/C_s)$, where n^0 is the water adsorption capacity at the feed gas condition, and C_g and C_s are the heat capacities of the feed gas and the zeolite, respectively (62,63). In this case, the bed temperature at the trailing edge of the water MTZ remains equal to the temperature of the feed gas.

The basic step of a PSA gas drying process using zeolites are:

1. Adsorption of the trace or dilute (< 5 mol %) water vapor from a feed gas at an elevated pressure (30–200 psig) by flowing the gas over a zeolite bed and withdrawing a dry product gas at the pressure of the feed gas
2. Countercurrent depressurization of the adsorber to near-ambient pressure and venting the effluent gas
3. Countercurrent purging of the bed at a near-ambient pressure with a part of the dry product gas from step 1 and discarding the effluent gas
4. Countercurrent repressurization of the adsorber with a part of the dry product gas from step 1

The cycle is then repeated (64). Adsorption at lower feed gas pressure (5–10 psig) and depressurization under vacuum (simultaneous evacuation and purging with dry product

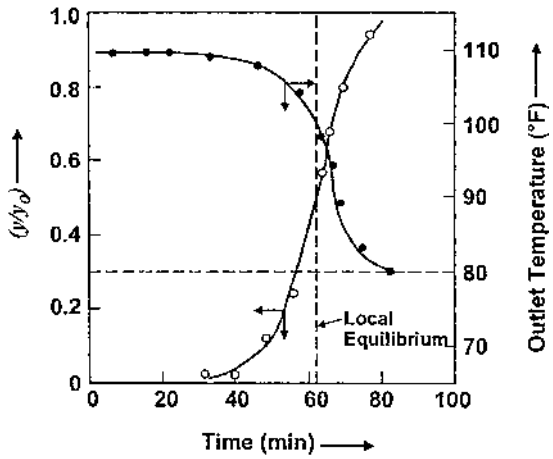

Fig. 20 Nonisothermal breakthrough curves for type II column dynamics: trace water adsorption from air on 4A zeolite at 26.7°C.

gas) are also possible operations (22,64). Figure 21 is a schematic diagram of a two-bed Skarstrom-type PSA dryer that can be operated with the above cycle. The typical total cycle time for all steps of a PSA dryer is 2–15 min.

Operating between the adsorption and desorption pressures of 7.8 and 1.0 atm, respectively, a PSA dryer containing 4A zeolite could produce a dry air stream with a dew point of −55°C (65). Lowering the desorption pressure to 0.65 atm could reduce the product gas dew point to −67°C (65). A critical variable for a PSA dryer is the ratio of the actual volume of purge gas to feed gas per cycle. Increasing this ratio increases product purity at the expense of reduced product recovery.

A zeolitic PSA process for removal of bulk water (10–20 mol %) from an alcohol vapor mixture called "adsorptive heat recovery system" was designed for breaking water-alcohol azeotropes (66,67). The feed gas was heated to 120–230°C to prevent condensation. Desorption was achieved by back purging the zeolite bed at feed gas conditions with a noncondensable dry gas (nitrogen). The purge effluent was cooled to condense the water vapor and then recycle the nitrogen. This process saved energy by preserving the energy of adsorption of water inside the zeolite bed at the end of the adsorption step, unlike the typical gas drying process. Figure 22 shows the water concentration in the effluent gas during the adsorption step of the process (66). This behavior is called type 1 adsorption column dynamics (62,63) and is favored when $(n^0/y^0) < (C_g/C_s)$. The trailing edge of the water MTZ is at an elevated temperature for this case.

Zeolites are also used for many special drying applications. 3A zeolites are used for drying polar gases like alcohols, amines, and H_2S because they are highly selective molecular sieves for water; the other polar components cannot enter and compete with water on the polar zeolitic adsorption sites (68). Similarly, 3A zeolites are preferred for drying reactive gases like olefins, diolefins, and acetylenic hydrocarbons because these gases are excluded from entering the zeolite pores where they can polymerize (68). Acid-resistant zeolites such as mordenite and chabazite (with high Si/Al ratio) are used for drying acidic gases such as HCl, HNO_3, SO_2, and NO_2 (67,68).

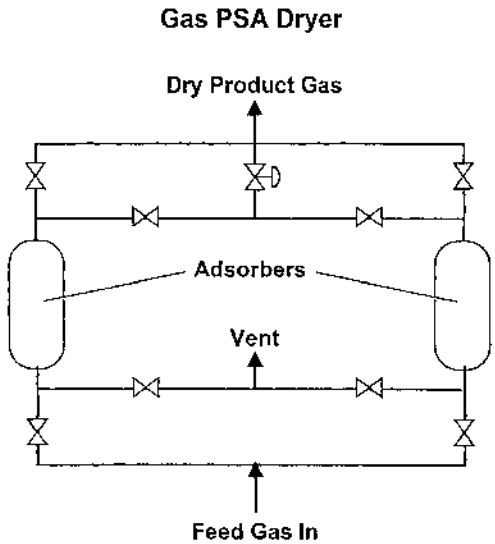

Fig. 21 Schematic diagram of a two-bed PSA dryer.

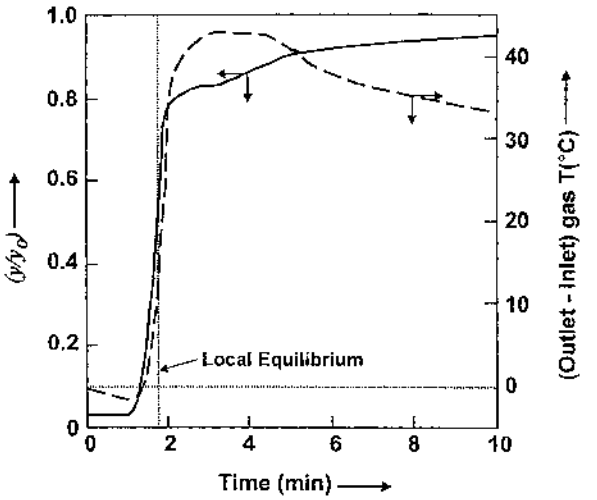

Fig. 22 Nonisothermal breakthrough curves for type I column dynamics: water adsorption from alcohol vapor on zeolite.

Various adsorber designs are used as zeolitic dryers. These include the conventional vertical adsorber with the vessel length/diameter ratio > 1, horizontal adsorbers with the vessel length/diameter ratio < 1 (69), radial bed adsorbers in which the adsorbent is packed in an annular section between two coaxial cylinders (69), and rotary bed adsorbers in which a shallow wheel-shaped adsorbent layer (honeycomb-shaped alumina substrate coated with a zeolite) turns about an axis and a section of the wheel is fed continuously with the wet feed gas while another section is continuously regenerated by heating (70).

B. Production of Oxygen-Enriched Air

A large variety of PSA process concepts have been developed for direct production of (23–95) mol % oxygen from ambient air using various ion-exchanged forms of zeolites of type A, X, and mordenite (23). Some of these concepts are called vacuum swing adsorption (VSA) because the final desorption pressure is subatmospheric.

The zeolites currently favored for air separation are LiX (or Li-LSX) families because of their isotherm shapes for nitrogen adsorption shown by Fig. 4a: relatively low nitrogen adsorption capacity at lower partial pressures and high nitrogen adsorption capacity at higher partial pressures, a profile which offers the highest N_2 adsorption working capacity for a PSA/VSA system. Also, LiX zeolites have low to moderate heats of adsorption for nitrogen and oxygen (see Table 9). These properties, in combination, result in a lower bed size factor (BSF = ratio of amount of adsorbent to amount of product gas per cycle), a higher oxygen recovery from air feed, and a lower specific energy of separation, all of which are desirable design characteristics.

For example, a VSA process consisting of six steps (71)

1. Pressurizing the adsorber from an intermediate pressure level to the final adsorption level (P_A) by introducing compressed air feed
2. Flowing compressed air feed through the adsorber to produce the oxygen-enriched product gas at P_A

3. Countercurrently depressurizing the adsorber to ambient pressure and venting the effluent gas
4. Countercurrently evacuating the adsorber to a subatmospheric pressure level (P_D)
5. Countercurrently purging the adsorber at pressure P_D with a part of the oxygen-enriched product gas while venting the effluent gas
6. Countercurrently pressurizing the adsorber from P_D to the intermediate pressure level with a part of the oxygen-enriched product gas from step 2.

produces a 90 mol % oxygen-enriched product gas (dry and free of carbon dioxide) with an oxygen recovery of 53% from the air feed (71). The adsorbent used was LiX and the adsorption (P_A) and desorption pressures were 1.43 and 0.34 atm, respectively. The mean adsorbent temperature was 290 K and the total cycle time was 70 s. The BSF was 830 pounds of zeolite per TPD (tons per day) of oxygen. The total power requirement was 11.6 kW per TPD oxygen when the product gas was delivered at 6.45 atmospheres by recompression (71).

Table 13 shows the results of a comparative study of various zeolites for production of 90 mol % oxygen from air by a VSA process where P_A and, P_D were 1.48 and 0.25 atm, respectively, and the feed gas temperature was at least 300 K (72). The superiority of LiX zeolite is evident.

Figure 23 demonstrates the effects of the mean pore size of the binder material of a Li-LSX zeolite on the performance of a VSA oxygen process operating between P_A and P_D levels of 1.40 and 0.33 atm, respectively, at a base temperature of 298 K (24). Both the oxygen production rate (m^3/h of oxygen per ton of zeolite) and the oxygen recovery from air (%) increased with the diameter of the binder pores. This implies that gas flow resistance in the mesopores and macropores of the binder is the controlling mechanism for mass transfer, as discussed previously.

Zeolitic PSA processes have also been designed to produce a relatively low-purity oxygen-enriched gas (23–30 mol % oxygen) directly from ambient air (23). One of these processes is a three-step cycle (73):

1. Pressurizing the adsorber cocurrently with compressed air to pressure P_A without any withdrawal of gas
2. Cocurrently depressurizing the adsorber to an intermediate pressure level while producing an oxygen-enriched product gas
3. Countercurrently depressurizing the adsorber to ambient pressure and venting the effluent gas (73)

Figure 24 describes the performance of this "Oxyrich process" using three different zeolites (NaX, 5A, and Na-mordenite) and a P_A value of 3.72 atm (74). The feed air temperature was 294 K. A large oxygen production capacity and oxygen recovery can be

Table 13 Comparative Performance of Various Zeolites for Production of 90% Oxygen from Air by a VSA Process

Zeolite	BSF	Energy of separation
NaX	1.00	1.00
CaX	1.28	1.78
LiX	0.51	0.88

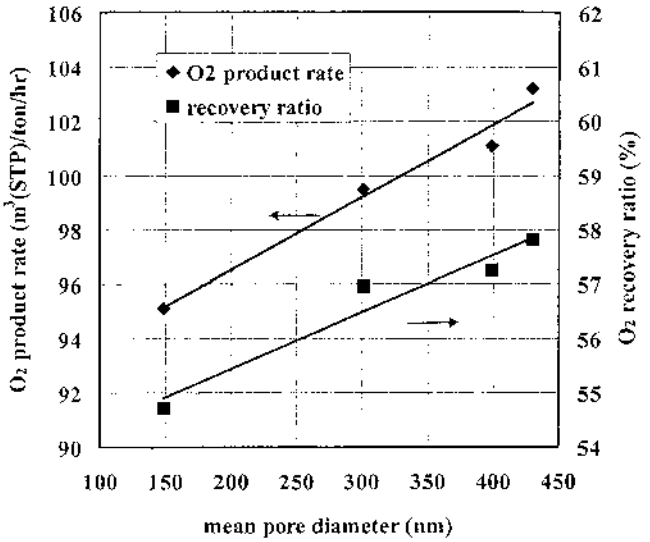

Fig. 23 Performance of a VSA process for production of 90% oxygen from air using LiLSX zeolite as a function of mean pore size of the zeolite binder phase.

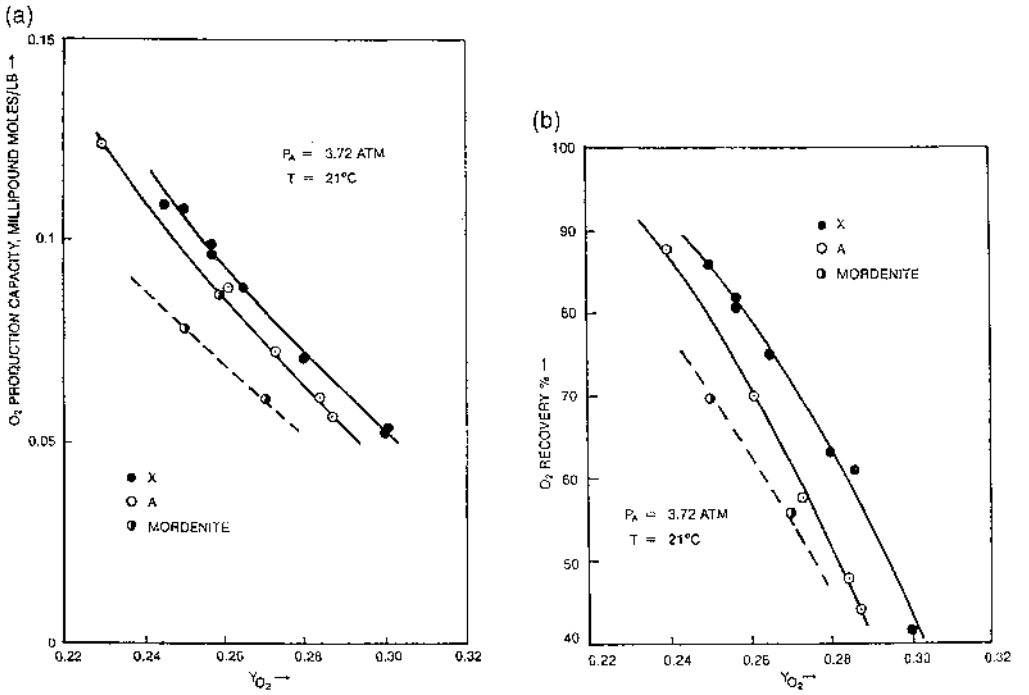

Fig. 24 Performance of a PSA process for direct production of low-purity oxygen from air by various zeolites: (a) oxygen productivity; (b) oxygen recovery from air.

achieved by this simple PSA process. The zeolite ranking for the performance of the process was NaX > 5A > Na-mordenite because nitrogen was most weakly adsorbed and therefore easiest to desorb on the NaX zeolite under the very mild conditions of desorption used by the process (no product back purge or evacuation). This example illustrates the importance of the desorption characteristics of a zeolite for any PSA/VSA process. The NaX zeolite performed best even though it had a lower nitrogen capacity and lower selectivity of adsorption for nitrogen relative to oxygen than the other samples.

Rapid pressure swing adsorption (RPSA) has been developed for the production of low-purity oxygen enriched air (25–50 mol % oxygen). RPSA processes with a total cycle time of seconds can increase the oxygen productivity per unit amount of zeolite by orders of magnitude compared to the conventional cycles (23). Figure 25 shows a schematic diagram of an RPSA process design that uses two or more layers of a zeolitic adsorbent inside a single adsorption vessel (75). The layers are separated by a flow-restricting screen. The steps of this RPSA cycle are:

1. Simultaneous pressurization to a pressure of P_A with compressed air and adsorption of nitrogen
2. Simultaneous depressurization to ambient pressure and back purge with a part of the oxygen-enriched product gas generated by the companion layer

Figure 26 shows the performance of this RPSA process using NaX zeolite (0.5-mm) beads at feed air pressure of 2.2–3.1 atm. The total cycle time was 12 s(76). Very high oxygen production capacity and recovery from air can be achieved when the oxygen product purity is less than 40 mol %. This process was found to be superior in performance over other RPSA process designs for low-purity oxygen product even though the other processes were operated at a faster frequency (23). Low-purity oxygen-enriched air is useful for enhanced combustion in metallurgical furnaces and cupolas (77).

RPSA cycles require smaller zeolite particles to achieve faster adsorption kinetics. However, large pressure drops are developed when the gas flow rates are high. Zeolite monoliths offer very low pressure-drops and are resistant to attrition. Recent air separation studies with square lattice channel monoliths prepared from 5A zeolite powder and Na-bentonite binder exhibited inferior separation performance compared to a packed bed due to channeling at high flow rates and early breakthrough of nitrogen

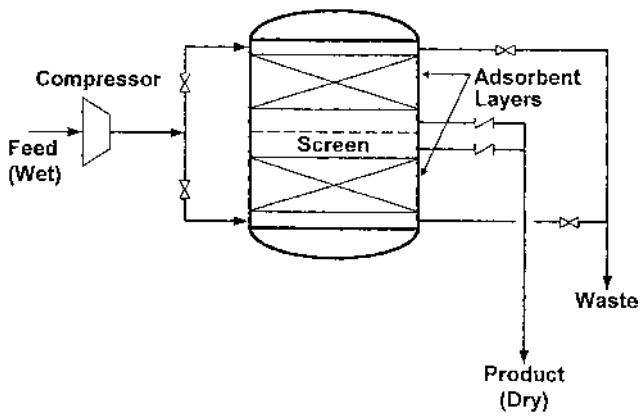

Fig. 25 Schematic diagram of a single-bed rapid-pressure-swing-adsorption (RPSA) unit.

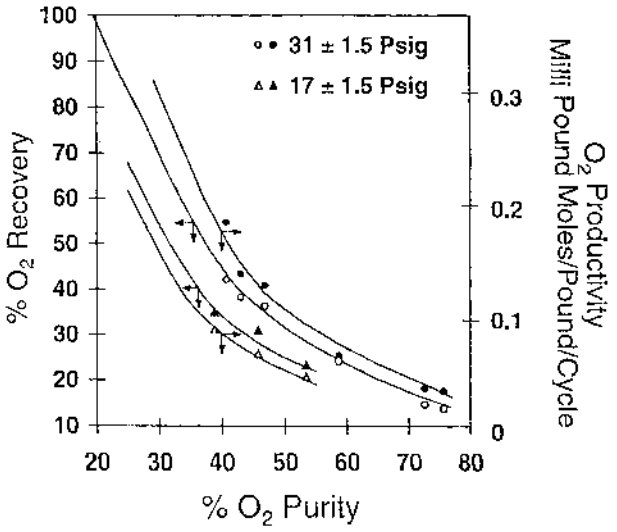

Fig. 26 Performance of a RPSA process for production of oxygen-enriched air using 5A zeolite.

(78,79). Further development is needed to make monolith designs competitive with conventional pelletized columns.

C. Simultaneous Production of Nitrogen and Oxygen From Air

Several VSA processes have been developed for simultaneous production of about 90 mol percent oxygen and 99+ mol % nitrogen-enriched gases from ambient air (23). One four-step process consists of (80,81):

1. Flowing ambient air at near ambient pressure (P_A) through a zeolite bed and withdrawing a 90+ mol % oxygen-enriched product gas
2. Cocurrently rinsing the adsorber at pressure P_A with a stream of nearly pure nitrogen and withdrawing a dry, CO_2-free air-like effluent gas for rejection or for recycling as feed gas
3. Countercurrently evacuating the adsorber to a subatmospheric pressure level P_D while withdrawing a 99+ mol % nitrogen-enriched gas, a part of which is withdrawn as product gas and the balance is used in step 2.
4. Countercurrentiy pressurizing the adsorber from P_D to P_A with a part of the oxygen-enriched product gas from step 1.

Table 14 summarizes the performance of this process using Na-mordenite as the adsorbent (23). The data are for the case where the effluent gas from step 2 was not recycled.

A variation of this VSA process eliminates step 2 (82). Instead, the gas evacuated in step 3 is divided into two parts: the first part, which is lean in nitrogen, is rejected. The second part, which has an average nitrogen composition of more than 95 mol %, is withdrawn as product. Figure 27 shows a schematic flowsheet for this process. This simple three-step process called the "fractionated VSA process" requires that the nitrogen selectivity of the zeolite over oxygen be high (>8) so that a highly nitrogen-enriched desorbed gas is produced in the second part of the evacuation step from a column which is initially saturated with air, which is the condition after step 1 (23,83). The performance of this process using CaX zeolite, which has a selectivity of about 11 for nitrogen over oxygen, is also given in Table 14. Use of CaX eliminates the need for the nitrogen rinse step required

Table 14 Comparative Performance of Various PSA Processes for Simultaneous Production of Nitrogen and Oxygen from Air

Process	Adsorbent	Operating pressure		Nitrogen product			Oxygen product		
		P_a (atm)	P_d (atm)	Purity (%)	Recovery (%)	Productivity[a]	Purity (%)	Recovery (%)	Productivity[a]
4-Step VSA	Na-mordenite	1.05	0.07	99.9	53.2	0.21	90.0	58.8	0.067
3-Step VSA	CaX	1.10	0.09	99.0	30.0	0.17	90.0	24.2	0.04
				98.0	42.6	0.25			

[a] Millipoundmoles per pound of zeolite per cycle.

by Na-mordenite for production of highly enriched nitrogen gas. These two processes demonstrate the versatility that can be achieved by matching the adsorptive properties of the zeolites with the process design to reach the same separation goal.

A key feature of all zeolitic air separation processes is that the water and the carbon dioxde impurities must be removed from the air feed before the air fractionation can be carried out (see Fig. 16). This is generally done in the same adsorber using a layer of a zeolitic or alumina desiccant stacked above the main zeolite layer for the air separation. NaX and 5A are frequently used for this purpose. The desiccant is cyclically regenerated by pressure reduction and countercurrent purging with the dry, CO_2-free desorbed gases from the main bed for the air separation. Often the conditions of operation of a PSA/VSA cycle are dictated by the conditions necessary for H_2O and CO_2 removal. The desiccant and the main zeolite layers generally operate with a residual amount of adsorbed molecules at the cyclic steady state.

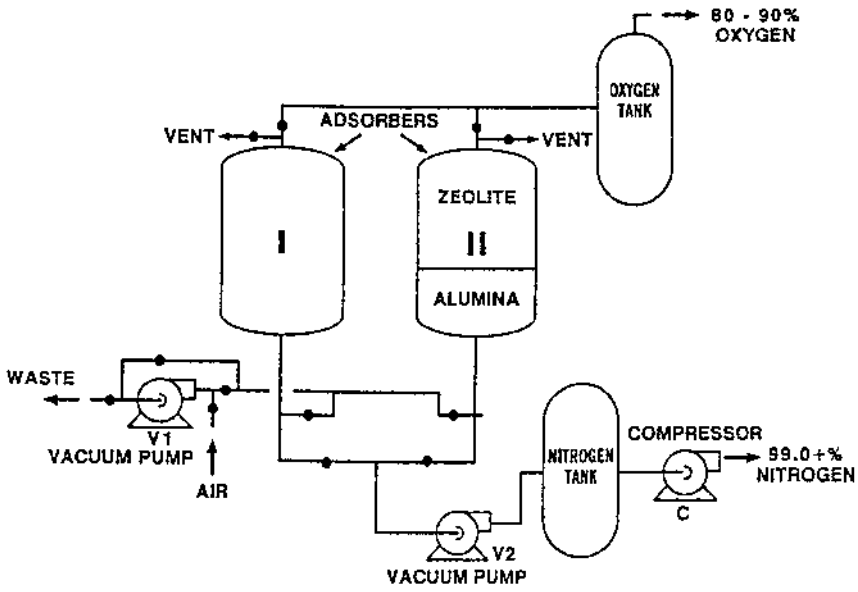

Fig. 27 Schematic diagram of a two-bed VSA process for simultaneous production of oxygen- and nitrogen-rich gases from ambient air.

D. Production of Hydrogen from SMR Off-Gas

The effluent gas from a steam-methane reformer (SMR) reactor, after passing through a water-gas shift reactor, typically contains 70–80% H_2, 15–25% CO_2, 3–6% CH_4, 1–3% CO (mol % on a dry basis), and trace amounts of N_2 at a pressure of 8–28 atm and a temperature of 21–38C (25). This gas is fed to a multicolumn PSA system for the production of 99.999+ mol % H_2 product gas at a pressure close to that of the feed gas. Numerous PSA process schemes have been developed (25). PSA processes have also been developed for simultaneous production of CO_2 and H_2 products from the SMR off-gas (84,85) and for direction production of ammonia synthesis gas with or without a CO_2 byproduct (86–88).

A popular nine-step PSA process for production of hydrogen is (89):

1. Flowing the feed gas at superatmospheric pressure (P_A) through an adsorber and withdrawing nearly pure H_2 product gas at P_A;
2. Cocurrently depressurizing the adsorber to an intermediate pressure while still producing a high-purity H_2 gas at the intermediate pressure;
3. Further cocurrently depressurizing the adsorber to a still lower pressure and producing another high-purity H_2 gas;
4. Again cocurrently depressurizing the adsorber to an even lower pressure and producing yet another stream of H_2-rich gas;
5. Countercurrently depressurizing the adsorber to near ambient pressure and venting the effluent gas;
6. Countercurrently purging the adsorber with hydrogen produced by step 4;
7. Countercurrently pressurizing the adsorber with the effluent gas from step 3;
8. Further pressurizing the adsorber countercurrently with the gas from step 2;
9. Countercurrently pressurizing the adsorber to pressure P_A using a part of the H_2 product gas generated by step 1.

The cycle is then repeated. Figure 28 shows a schematic flow diagram for this concept called "polybed process" employing 9 parallel adsorbers (89).

The adsorbers are packed with a layer of an activated carbon in the feed end and with a layer of 5A zeolite at the product end. Operating at a feed gas pressure of 20.7 atm

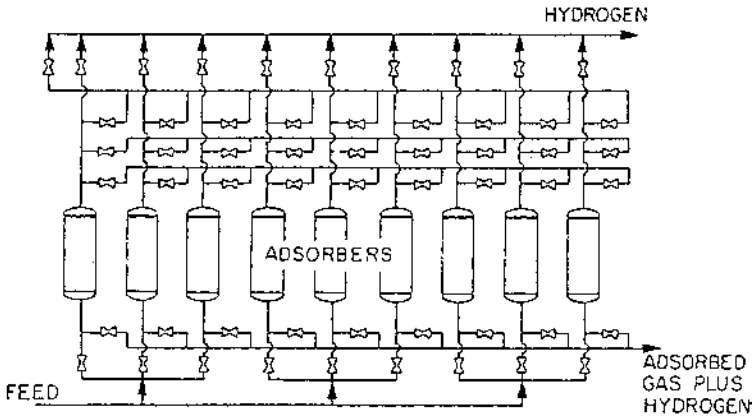

Fig. 28 Schematic diagram of a 9-bed PSA process for production of hydrogen from steam-methane reformer off-gas.

and at a temperature of 294 K, the process can produce 99.999+% pure H_2 with a recovery of 86% from the feed gas. The H_2 production capacity is about 35 ft^3 (1 atm, 15C) per cubic foot of adsorbent per cycle.

The activated carbon layer removes the H_2O, CO_2, and most of the CH_4 impurities from the feed gas. The balance of impurities are removed in the zeolite layer. The CO_2 removal is accomplished in the carbon bed even though zeolite 5A has a much high capacity and selectivity for CO_2. However, the strong adsorption of CO_2 by the zeolite makes its desorption (regeneration) unfavorable. Figure 29 shows the equilibrium-controlled desorption characteristics of CO_2 from a carbon (BPL) and a zeolite (5A) bed which is initially saturated with pure CO_2 at 1 atm and 303 K by purging with pure H_2 at the same conditions (25). It is apparent that efficient removal of CO_2 from the zeolite by H_2 purge, which is the main desorption mechanism for the PSA process, will require a very large quantity of H_2 and thus reduce its recovery. The desorption of CO_2 from BPL carbon is relatively easy; therefore, carbon is the preferred adsorbent for CO_2 removal.

Figure 30 shows the corresponding desorption characteristics of CO and N_2 by H_2 purge (25). Desorption of these gases is also easier from carbon than from the zeolite, but the zeolite bed can be cleaned reasonably well (70–80 mol % of impurities removed) without consuming a large quantity of H_2 product. This property, combined with the higher CO-H_2 and N_2-H_2 selectivities on the zeolite (see Table 7), and the larger adsorption capacities of polar CO and N_2 on the zeolite, make it the preferred adsorbent for the PSA process for H_2 production. The relatively higher N_2-H_2 selectivity on the zeolite is the key requirement for delivering a very-high-purity nitrogen-free H_2 product gas by the PSA process.

E. Production of Methane and Carbon Dioxide From Landfill Gas

Typical landfill gas contains equimolar amounts of CH_4 and CO_2 (dry basis) in conjunction with a variety of trace impurities (90). A PSA/VSA process called "Gemini 5" was developed for simultaneous product of 98+ mol % CH_4 and 98+ mol % CO_2

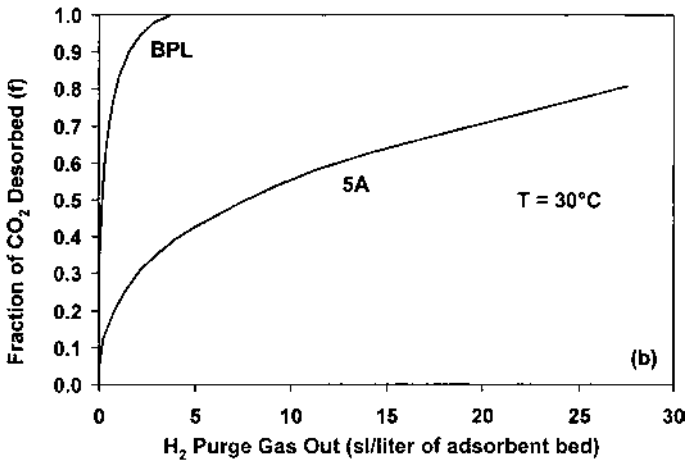

Fig. 29 Desorption characteristics of carbon dioxide from 5A zeolite and BPL carbon by purging with hydrogen at 30°C and 1 atm.

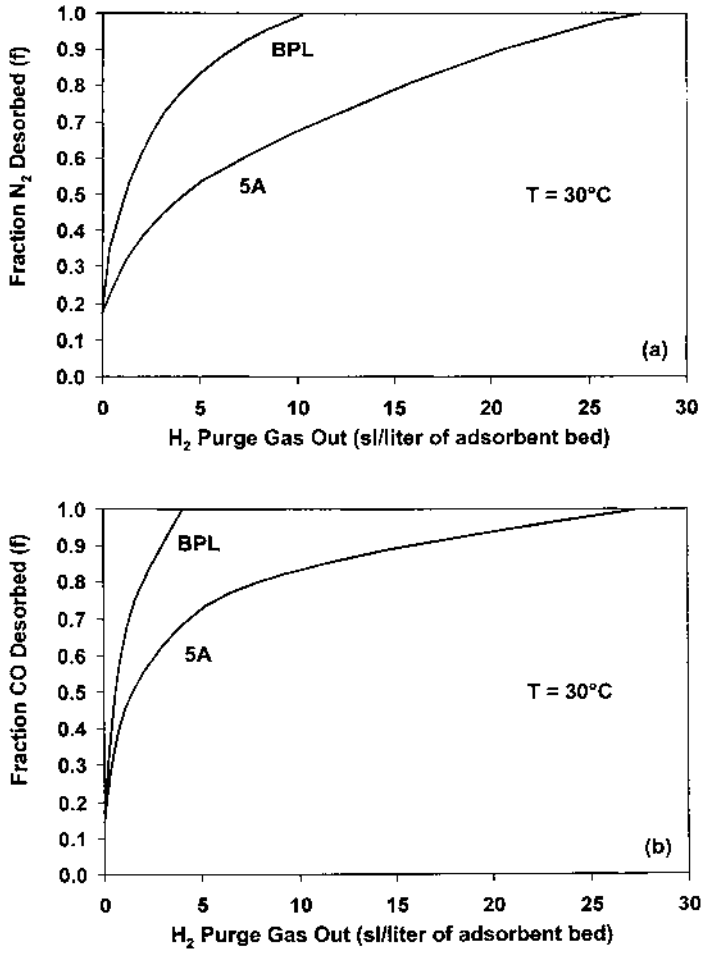

Fig. 30 Desorption characteristics of (a) carbon monoxide and (b) nitrogen from 5A zeolite and BPL carbon by purging with hydrogen at 30°C and 1 atm.

streams from landfill gas with 99% recovery of both components using a zeolite adsorbent. The process has five steps (91):

1. Adsorption of CO_2 on the zeolite from a compressed landfill gas to produce 98+ mol % CH_4-enriched product at the feed pressure (P_A);
2. Cocurrent CO_2 rinse of the adsorber at feed pressure with recycle of the effluent gas by mixing it with fresh feed gas;
3. Countercurrent depressurization of the adsorber to ambient pressure to produce a 98+ mol % CO_2 stream to be used in step 2;
4. Countercurrent evacuation of the adsorber to a subatmospheric pressure of P_D and withdrawal of the effluent gas as 98+ mol % CO_2 product;
5. Countercurrent repressurization of the adsorber from P_D to P_A by a part of the CH_4 product gas generated in step 1.

The cycle is then repeated. The process is capable of splitting a landfill gas containing 57% CH_4 and 43% CO_2 at a feed gas pressure of 6–12 atm into two highly enriched

products (98% CO_2 and 98% CH_4) using a proprietary X-type zeolite. The final desorption pressure was 0.07–0.26 atm (91).

Use of the zeolite for selective adsorption of CO_2 from CH_4 is justified because the method of adsorbent regeneration is different (pressure reduction and evacuation without CH_4 back purge) from the polybed process described in the previous section. The use of zeolite for CO_2-CH_4 separation in this case provides high capacity and selectivity for CO_2 without paying any penalty for CH_4 recovery. This process is a typical example of the judicious marriage of zeolite properties and process design for achieving a specific separation goal.

F. Separation of Normal and Isoparaffins

The 5A zeolite offers excellent steric selectivity for adsorption of normal paraffins over isoparaffins and cyclic hydrocarbons by excluding branched chain and ring compounds from entering the zeolite pores. This property has been used extensively by many corporations to design vapor phase adsorptive cycles for separation of normal and isoparaffins present in a variety of petroleum fractions (9,17,92). These processes are run at temperatures high enough to prevent condensation of the hydrocarbons but low enough to prevent chemical degradation.

The desorption of the normal paraffins from the 5A zeolite is performed in various ways. Vacuum desorption and purging the adsorber with an inert gas are practical methods when the paraffins have low carbon numbers and are not strongly adsorbed (93). Desorption schemes based on displacement by ammonia and lighter normal paraffins are employed when the feed mixture consists of heavy normal paraffins (94,95). The desorbing fluid is separated from the normal and isoparaffin-rich streams by distillation and recycled.

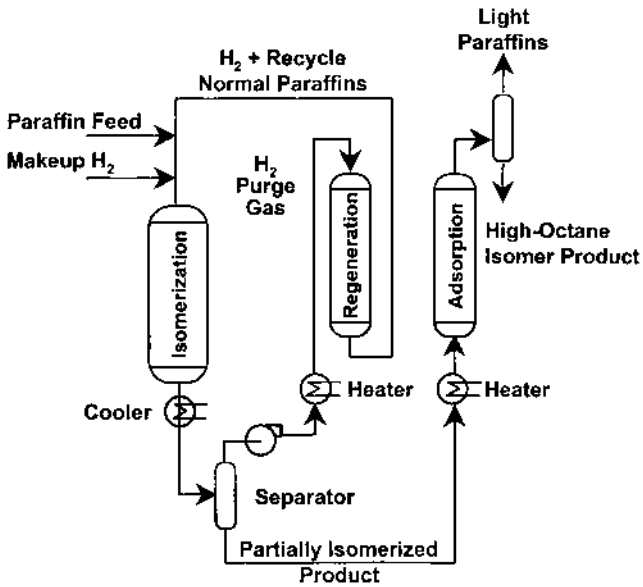

Fig. 31 Schematic flow diagram of a process integrating isomerization reactor and adsorptive paraffin-isoparaffin separation unit.

One of these adsorptive separation concepts called the "isosiv" process has also been integrated with the operation of an isomerization reactor in order to drive the equilibrium-controlled reaction to completion (96). A schematic flow diagram for total isomerization process is given in Fig. 31.

VIII. EPILOGUE

The examples of gas separation and purification applications cited above demonstrate the versatility and flexibility of process designs using zeolitic adsorbents and some of the ingenious designs developed to exploit the properties of zeolites to achieve a specific separation goal. The wide range of properties exhibited by zeolites encourages the development of new processes with the zeolitic material optimally matched to the separation task. Commercially successful applications of zeolites to separations of mixtures are expected to grow in the future, especially for supercritical or close-boiling liquid mixtures that are poor candidates for separation by distillation.

REFERENCES

1. S Sircar. Adsorption 6:359–365, 2000.
2. S Sircar. Applications of gas separation by adsorption for the future. Ads Sci Tech 19:347–365, 2001.
3. D W Breck. Zeolite Molecular Sieves. Malabar, FL; Krieger 1984.
4. R Szostak. Handbook of Molecular Sieves. New York: Van Nostrand Reinhold, 1992.
5. A Dyer. Introduction to Zeolite Molecular Sieves. New York: John Wiley, 1988.
6. JB Nagy, P Bodart, I Hannus, I Kiriesi. Synthesis, Characterization and Use of Zeolitic Microporous Materials. Szeged, Hungary: Decagel Ltd., 1998.
7. RM Barrer. Zeolites and Clay Minerals as Sorbents and Molecular Sieves. London: Academic Press, 1978.
8. AL Kohl, RC Riesenfield. Gas dehydration and purification by adsorption. In: Gas Purification. Houston, TX: Gulf Publishing, 1979, chapter 12, pp 574–656.
9. GE Keller, RA Anderson, CM Yon. Adsorption. In: Handbook of Separation Process Technology. New York: John Wiley, 1987, chapter 12, pp 644–696.
10. JD Sherman, CM Yon. Adsorption gas separation. In: Kirk Othmer Encyclopedia of Separation Technology, Vol. 1. New York: John Wiley, 1997, pp 129–172.
11. JL Humphrey, GE Keller. Adsorption. In: Separation Process Technology. New York: McGraw-Hill, 1997, chapter 4.
12. TC Golden, S Sircar. J Colloid Interf Sci 162:182–188, 1994.
13. MS Sun, O Talu, DB Shah. J Phys Chem B 100: 17276–17280, 1996.
14. MS Sun, O Talu, DB Shah. AIChE J 42:3001–3007, 1996.
15. MS Sun, D B Shah, H H Xu, O Talu. J Phys Chem B 102:1466–1473, 1998.
16. DH Olson, US Patent 6,488,741 (2002).
17. DM Ruthven. Principles of Adsorption and Adsorption Processes. New York: John Wiley, 1984.
18. J Kärger, DM Ruthven. Diffusion in Zeolites and Other Microporous Solids. New York: John Wiley, 1992.
19. S Sircar. I&EC Res 38:3670–3682, 1999.
20. DP Valenzuela, AL Myers. Adsorption Equilibrium Data Handbook. Englewood Cliffs, NJ: Prentice-Hall, 1989.
21. DM Young, AD Crowell. Physical Adsorption of Gases. London: Butterworths, 1962.
22. S Sircar. Drying processes. In: F Schüth, KSW Sing, J Weitkamp, eds, Handbook of Porous Solids, Vol. 5. Weinheim: Wiley-VCH, chapter 6.3, pp 2533–2567, 2002.

23. S Sircar, MB Rao, T C Golden. Fractionation of air by zeolites. In: Studies in Surface Science and Catalysis, Vol. 120. Amsterdam: Elsevier, 1998, pp 395–423.
24. S Hirano, S Yoshida, A Harada, S Morishita, E Furuya. Dynamic adsorption properties of Li ion exchanged zeolite adsorbents. In: K Kaneko, H Kanoh, Y Hanzawa, eds. Fundamentals of Adsorption, Vol. 7. Chiba City, Japan: IK International, 2002, pp 872–879.
25. S Sircar, TC Golden. Sep Sci Technol, 35:667–687, 2000.
26. R Kumar, S Sircar. Chem Eng Sci, 41:2215–2223, 1986.
27. S Sircar, MB Rao. AIChE J, 45:2657–2661, 1999.
28. S Sircar, AL Myers. Ads Sci Tech., 2:69–87, 1985.
29. JF Kirner. U.S. Patent 5,268,023 (1993).
30. RV Jasra, NV Choudary, SGT Bhat. I&EC Res 35:4221–4229, 1996.
31. O Talu, I Zwiebel. AIChE J 32:1263–1276, 1986.
32. AL Myers. AIChE J 48:145–160, 2002.
33. AL Myers, PA Monson. Langmuir 18:10261–10273, 2002.
34. MB Rao, S Sircar. Langmuir, 15:7258 7267, 1999.
35. AL Myers, JM Prausnitz. AIChE J., 11:121–127, 1965.
36. S Sircar. AIChE J 41:1135–1145, 1995.
37. S Siperstein, AL Myers. AICHE J 47:1141–1159, 2001.
38. CM Yon, PH Turnock. AIChE Symp Ser No 117, 67:75–83, 1971.
39. JA Dunne, R Mariwala, MB Rao, S Sircar, RJ Gorte, A L Myers. Langmuir 12:5888–5895, 1996.
40. JA Dunne, MB Rao, S Sircar, RJ Gorte, AL Myers. Langmuir 12:5896–5904, 1996.
41. JA Dunne, MB Rao, S Sircar, RJ Gorte, AL Myers. Langmuir 13:4333–4041, 1997.
42. S Sircar, RJ Mohr, C Ristic, MB Rao. J Phys Chem B 103:6539–6546, 1999.
43. DV Cao, S Sircar. I&EC Res, 40:156–162, 2001.
44. DV Cao, S Sircar. Ads Sci Tech 19:887–894, 2002.
45. RM Barrer, B Coughlan. Molecular Sieves. London: Society of Chemical Industry, 1968.
46. S Sircar, MB Rao. Heats of adsorption of pure gas and multi-component gas mixtures. In: JA Schwarz, CI Contescu, eds. Surfaces of Nanoparticles and Porous Materials. New York: Marcel Dekker, 1999, pp 501–528.
47. M Bülow, P Struve, S Pikus. Zeolites 2:267–270, 1982.
48. RM Rynders, MB Rao, S Sircar. AIChE J 43:2456–2470, 1997.
49. RJ Mohr, D Vorkapic, MB Rao, S Sircar. Adsorption 5:145–158, 1999.
50. DV Cao, RJ Mohr, MB Rao, S Sircar. J Phys Chem B, 104:10498–10501, 2000.
51. D Paschek, R Krishna. Chem Phys Lett 333:278, 2001.
52. J Caro, M Bülow, W Schirmer, J Kärger, W Heink, H Pfeifer. J Chem Soc Faraday Trans I, 81:2541–2550, 1985.
53. J Kärger, H Pfeifer. Zeolites 7:91, 1987.
54. J. Habgood. Can J Chem 36:1384–1397, 1958.
55. J Izumi, M Suzuki. Adsorption 7:27–39, 2001.
56. S Sircar. J Chem Soc Faraday Trans I, 79:785–796, 1983.
57. S Sircar, JR Hufton. Adsorption, 6:137–147, 2000.
58. D Peterson. Influence of preadsorbed water on the sorption of N_2 by zeolites at ambient temperatures. In: WH Flank, ed. Adsorption and Ion Exchange with Synthetic Zeolites. Washington, DC: American Chemical Society Symposium Series No. 135, 1980, pp 107–122.
59. ND Hutson, SC Zajic, and RT Yang. I&EC Res 39:1775–1780, 2000.
60. JJ Collins. Chem Eng Progr Symp Ser 1:5, 1971.
61. JW Carter, DJ Barrett. Trans Inst Chem Eng 51:75–81, 1973.
62. CY Pan, D Basmadjian. Chem Eng Sci 25:1653–1664, 1970.
63. S Sircar. Dynamics of sorption in adiabatic columns. In: Fundamentals of Adsorption, Vol. 1. New York: Engineering Foundation, 1984, pp 585–596.
64. CN Skarstrom. U.S. Patent 2,944,627 (1960).
65. K Suzuki. Kemikaru Enjiniyaringu, 7:71–76, 1984.

66. DR Garg, CM Yon. Chem Eng Prog 82:54–60, 1986.
67. JP Ausikaitis. U.S. Patent 4,373,935 (1983).
68. GE Hales. Chem Eng Prog 67(11):49–53, 1971.
69. UV Gemmingen. Linde Report on Science and Technology, Vol. 54. Technical report, ACHEMA, 1990, pp 8–12.
70. T Hirose, T Kuma. Honeycomb rotor continuous adsorber for solvent recovery and dehumidification. In: The 2nd Korea-Japan Symposium on Separation Technology, 1990.
71. FW Leavitt. U.S. Patent 5,415,683 (1995).
72. FW Leavitt. U.S. Patent 5,074,892 (1991).
73. WC Kratz, S Sircar. U.S. Patent 4,685,939 (1987).
74. S Sircar, WC Kratz. Sep Sci Tech 23:437–450, 1988.
75. S Sircar. U.S. Patent 5,071,449 (1991).
76. S Sircar, BF Hanley. Adsorption 1:313–320, 1995.
77. S Sircar. Adsorption 2:323–326, 1996.
78. YY Li, SP Perera, BD Crittenden. Trans Inst Chem Eng 76:921–930, 1998.
79. YY Li, SP Perera, BD Crittenden. Trans Inst Chem Eng 76:931–941, 1998.
80. S Sircar, J Zondlo. U.S. Patent 4,013,429 (1977).
81. WP Schmidt, R Kumar, AD Abel. U.S. Patent 4,813,977 (1989).
82. S Sircar. U.S. Patent 5,084,075 (1992).
83. S Sircar. Sep Sci Technol 23:2379–2396 1988.
84. S Sircar. U.S. Patent 4,171,206 (1979).
85. S Sircar, WC Kratz. Sep Sci Technol 23:437, 1988.
86. A Fuderer. U.S. Patent 4,375,363 (1983).
87. S Sircar. U.S. Patent 4,813,980 (1989).
88. S Sircar. Sep. Sci. Technol 25:1087–1099 (1990).
89. A Fuderer, E Rudelsdorfer. U.S. Patent 3,986,849 (1976).
90. S Sircar, R Kumar, WR Koch, J Vansloun. U.S. Patent 4,770,676 (1988).
91. S Sircar. Sep Sci Technol 23:519–529, 1988.
92. CW Chi, WP Cummings. Adsorptive separation of gases. In: Kirk Othmer Encyclopedia of Chemical Technology, Vol. 1, 3rd ed. New York: Wiley-Interscience, 1978, pp 541–563.
93. RT Cassidy, ES Holmes. AIChE Symp. Ser. 233, 80:68–73, 1984.
94. DE Cooper, HE Griswold, RM Lewis, RW Stokeld. Chem Eng Prog 62:69–73, 1966.
95. WJ Aster, ML Campbell, WR Epperly, JL Robertson. Hydrocarbon Proc 48:134–138, 1969.
96. MF Symoniak. Hydrocarbon Proc 59:110–114, 1980.